

## Boron Carbide: Structure, Properties, and Stability under Stress

Vladislav Domnich, Sara Reynaud, Richard A. Haber, and Manish Chhowalla<sup>†</sup>

Department of Materials Science and Engineering, Rutgers, The State University of New Jersey, Piscataway, NJ 08854

**Boron carbide is characterized by a unique combination of properties that make it a material of choice for a wide range of engineering applications. Boron carbide is used in refractory applications due to its high melting point and thermal stability; it is used as abrasive powders and coatings due to its extreme abrasion resistance; it excels in ballistic performance due to its high hardness and low density; and it is commonly used in nuclear applications as neutron radiation absorbent. In addition, boron carbide is a high temperature semiconductor that can potentially be used for novel electronic applications. This paper provides a comprehensive review of the recent advances in understanding of structural and chemical variations in boron carbide and their influence on electronic, optical, vibrational, mechanical, and ballistic properties. Structural instability of boron carbide under high stresses associated with external loading and the nature of the resulting disordered phase are also discussed.**

### I. Atomic Structure, Stoichiometry, and Polytypism

THE atomic structure of boron carbide has been extensively discussed in the literature.<sup>1–8</sup> The primary structural units of boron carbide are the 12-atom icosahedra located at the vertices of a rhombohedral lattice of trigonal symmetry ( $R\bar{3}m$  space group), and the 3-atom linear chains that link the icosahedra along the (111) rhombohedral axis, as illustrated in Fig. 1. This structure can also be described in terms of a hexagonal lattice based on a nonprimitive unit cell, in which case the [0001] axis of the hexagonal lattice corresponds to the [111] rhombohedral direction (Fig. 1). The presence of icosahedra within the boron carbide structure is a consequence of elemental boron's ability to form caged structures of a variety of sizes<sup>5,9</sup>; the icosahedra in boron carbide are essentially two pentagonal pyramids bonded together.<sup>10</sup> As such, two types of chemically distinct sites, polar and equatorial, are possible within an individual icosahedron. The polar sites correspond to those atoms that link the icosahedra together. The polar atoms within the cage

are also the three atoms from each of the two planes opposite one another in the crystal structure. The equatorial sites on the other hand are those to which the 3-atom chains are bonded, and these sites form a hexagonal chair within the icosahedron (Fig. 1).

Information on the crystal symmetry of boron carbide is readily available from diffraction measurements; however, the exact site occupancies by carbon and boron atoms are still debated. This is due to the similarity in both electronic and nuclear scattering cross-sections for boron and carbon ( $^{11}\text{B}$  and  $^{12}\text{C}$  isotopes),<sup>11,12</sup> which makes it difficult to distinguish these two atoms by most characterization techniques. From the crystal symmetry considerations, two stoichiometries have been originally proposed as candidates for the stable phase of boron carbide: (i) the carbon rich  $\text{B}_4\text{C}$  (or  $\text{B}_{12}\text{C}_3$ ) compound, with the idealized structural configuration  $(\text{B}_{12})\text{CCC}$ ,<sup>13,14</sup> where  $(\text{X}_{12})$  represents the icosahedral atoms and XXX stands for the chain atoms, and (ii) the  $\text{B}_{13}\text{C}_2$  (or  $\text{B}_{6.5}\text{C}$ ) compound, described by an idealized  $(\text{B}_{12})\text{CBC}$  structural formula, where the center chain carbon atom is replaced by boron.<sup>15,16</sup> Formation of additional intermediate phases with crystal symmetry other than  $R\bar{3}m$ , such as a monoclinic modification of  $\text{B}_{13}\text{C}_2$ ,<sup>17</sup> has also been reported. These variations have been reflected in several versions of the B–C phase diagram reported in the literature<sup>18–23</sup>; Fig. 2 shows examples of the two more commonly used phase diagrams.<sup>20,21</sup> There is agreement in the community about the existence of a wide range of solid solubility for carbon in the stable phase and a homogeneous range extending from ~8 at.% C to ~20 at.% C,<sup>3,22–24</sup> although synthesis of a single crystal with the  $\text{B}_{3.2}\text{C}$  stoichiometry, corresponding to 24 at.% C has also been reported.<sup>25</sup> Beyond ~20 at.% C, a mixture of stable phase boron carbide and carbon is often encountered, which has a eutectic point at ~30 at.% C of 2350°C<sup>20</sup>; but the latter has also been debated to be as low as 2240°C.<sup>21</sup> Low carbon content phases (i.e. below 8 at.% C) are generally agreed to be solid solutions of the stable phase boron carbide and pure boron.

The rhombohedral lattice parameters for the carbon-rich  $\text{B}_4\text{C}$  compound are  $a = 5.16 \text{ \AA}$  and  $\alpha = 65.7^\circ$ , with minor variations depending on the extent of the investigation.<sup>2,13,14,26–33</sup> Converted into the more easily worked with hexagonal lattice parameters,  $\text{B}_4\text{C}$  has values of  $a_0 = 5.60 \text{ \AA}$ ,  $c_0 = 12.07 \text{ \AA}$ , and an axial ratio of  $c_0/a_0 = 2.155$ .<sup>3</sup> Due to the difference in atomic radii of carbon and boron, B-rich boron carbides have slightly expanded lattices. Using precision structural

D. J. Green—contributing editor

Manuscript No. 29735. Received May 25, 2011; approved August 27, 2011.  
<sup>†</sup>Author to whom correspondence should be addressed. e-mail: manish1@rei.rutgers.edu

# Feature

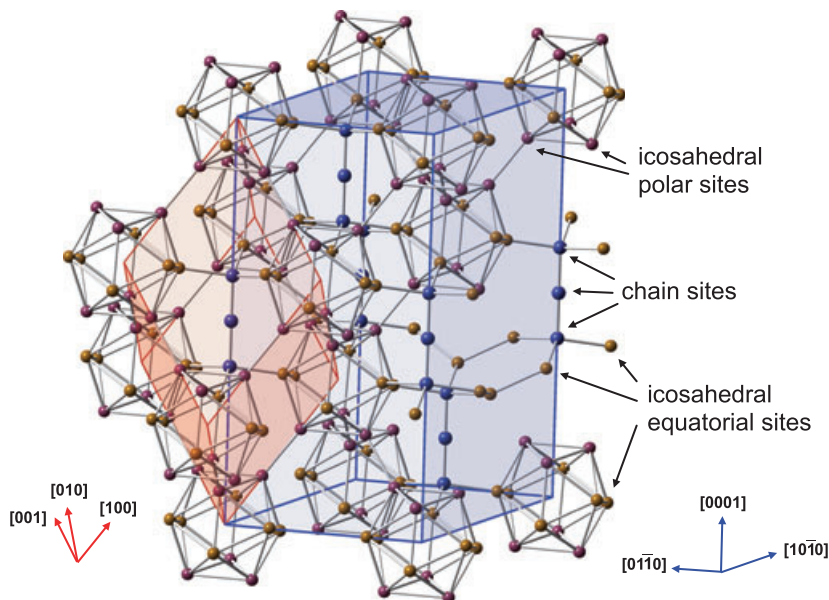


**Fig. 1.** Boron carbide lattice showing correlation between the rhombohedral (red) and the hexagonal (blue) unit cells. Inequivalent lattice sites are marked by arrows.

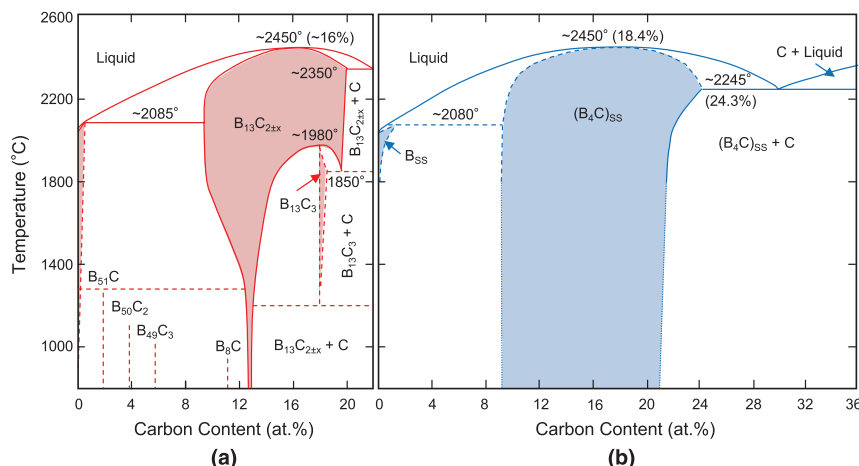


**Fig. 2.** Phase diagram of boron carbide after (a) Ekbom and Amundin,<sup>20</sup> depicting  $B_{13}C_2$  as the stoichiometrically stable phase and presuming the presence of several low temperature phases, and (b) Beauvy,<sup>21</sup> depicting the more widely accepted  $B_4C$  as the stoichiometrically stable phase, with solid solutions with B and C on each respective side.

characterization of high-purity boron carbides spanning the entire homogeneity range, Aselage *et al.* established a correlation between lattice parameters and stoichiometry.<sup>33</sup> As illustrated in Fig. 3(a), the  $a$  parameter experiences a steady increase toward more boron-rich stoichiometries, whereas a change in the slope at ~13 at.% C is observed for the compositional dependence of the  $c$  parameter. Further, neutron powder diffraction data<sup>11,34</sup> show that the chain bond length in boron carbides at 13 at.% C is reduced by 2%–3% compared to that in boron- and carbon-rich material [Fig. 3(b)]. These experimental observations can be understood in terms of the formation of an intermediate  $B_{6.5}C$  configuration and the change in the mechanisms for incorporation of carbon atoms into the lattice that occurs at 13.3 at.% C composition, as discussed below.

Despite the absence of experimental methods that can unambiguously pinpoint the positions of boron and carbon atoms in the lattice, various atomic configurations have been suggested for boron carbide based on theoretical modeling<sup>4,35-46</sup> and the available experimental data obtained by nuclear magnetic resonance,<sup>47-50</sup> neutron<sup>11,34,51</sup> and X-ray<sup>2,31-33,52</sup> diffraction, infrared<sup>30,53-56</sup> and Raman<sup>56-61</sup> spectroscopy, and X-ray absorption<sup>12</sup> and scattering<sup>62,63</sup> techniques. Possible combina-

tions of such structural elements as  $B_{12}$ ,  $B_{11}C$ ,  $B_{10}C_2$ , and  $B_9C_3$  icosahedra and CCC, CBC, CCB, CBB, BCB, and BBB chains, as well as the nonlinear chains that include four boron atoms and chains with vacancies, have been suggested in these studies.

The results of the theoretical energy minimization consistently indicate that the  $(B_{11}C)CBC$  structure is preferred to the  $(B_{12})CCC$  at the carbon-rich end of the homogeneity range.<sup>4,36,37,39,40,43-45,64</sup> Because of the existence of nonequivalent atomic positions within the icosahedra, two variants of  $(B_{11}C)CBC$  should be considered: the polar  $(B_{11}C^P)$  configuration, where one of the boron atoms in the icosahedron is substituted by carbon in the polar site, and the equatorial  $(B_{11}C^E)$  configuration, where the substitution occurs in the equatorial site. The polar configuration is found to be energetically preferred to the equatorial one in all studies where the two structures have been modeled within the same calculation framework.<sup>35,40,45,65</sup> It should be also noted that the substitution of carbon into the icosahedron induces small monoclinic distortions in the  $R\bar{3}m$  symmetry, amounting to 1.8% and 0.5% of the lattice parameter and to 1.0% and 0.1% of the rhombohedral angle for the polar and the equatorial configurations, respectively.<sup>39</sup>

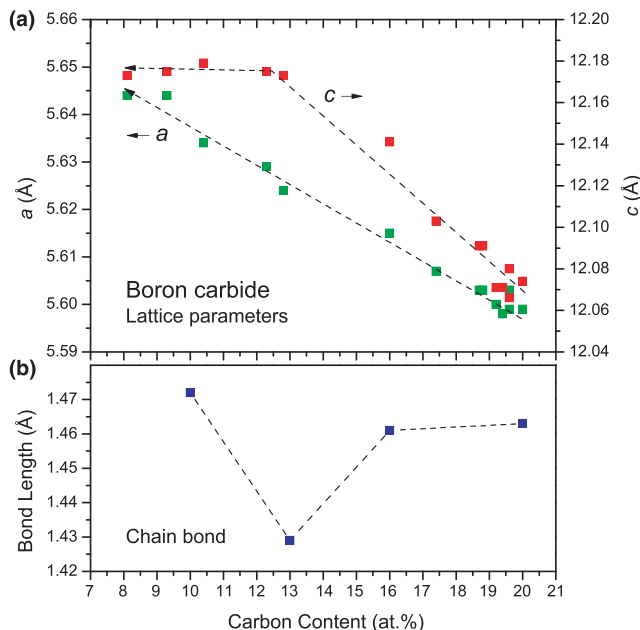


**Fig. 3.** Dependence of (a) hexagonal lattice parameters  $a$  and  $c$ , and (b) the chain bond length of boron carbide on carbon content. Lines serve as guides to the eye. Data from (a) X-ray diffraction measurements by Aselage *et al.*<sup>33</sup> and (b) neutron powder diffraction measurements by Morosin *et al.*<sup>11,34</sup>

From an experimental viewpoint, the possibility that  $(B_{11}C)CBC$  is the true structural representation of the  $B_4C$  stoichiometry was originally inferred,<sup>47</sup> and later corroborated,<sup>48,66</sup> by nuclear magnetic resonance (NMR) observations. However, concurrent NMR studies by other groups offered alternative interpretations, including structures with chains consisting only of carbon atoms,<sup>49</sup> and chains with two carbon atoms substituted by boron.<sup>50</sup> In part, these discrepancies stemmed from the lack of agreement on the assignment of specific NMR peaks to either the chain center C atom or to the C atom in the polar icosahedral site. Theoretical simulation of NMR spectra in  $(B_{11}C^P)CBC$ ,  $(B_{11}C^e)CBC$ , and  $(B_{12})CCC$  configurations based on density functional theory (DFT) helped to resolve this issue.<sup>64</sup> It was found that the best correlation between the theoretical and the experimental NMR spectra for the  $B_4C$  stoichiometry could be achieved for the  $B_4C$  structure consisting of all CBC chains and a mixture of  $(B_{12})$ ,  $(B_{11}C^P)$ , and  $(B_{10}C_2^P)$  icosahedra in the ratio of 2.5/95/2.5, with the two C atoms in the latter structure located in the antipodal polar sites.

In a related study that employed a similar modeling framework,<sup>39,65</sup> comparison of theoretically simulated and experimental Raman and infrared spectra of  $B_4C$  also implied that  $(B_{11}C^P)CBC$  is the true representation of boron carbide at this stoichiometry. Further, the presence of the boron atom in the  $B_4C$  chain has been inferred from X-ray<sup>2,31,32</sup> and neutron diffraction<sup>34,51</sup> data, owing to the observation of the lower scattering at the chain centers, and from X-ray absorption<sup>12</sup> and scattering<sup>62,63</sup> observations. Thus, the majority of theoretical and experimental investigations agree that  $(B_{11}C^P)CBC$  is the preferred atomic configuration for the  $B_4C$  stoichiometry.

It should be noted that even higher estimations for the carbon-rich edge of the homogeneity range have been discussed. Konovalikhin *et al.* reported successful synthesis of single crystal boron carbide with ~24 at.% C.<sup>25</sup> To account for higher carbon content in this compound, the proposed structural configuration included a distribution of CBC chains and  $(B_{11}C)$ ,  $(B_{10}C_2)$ , and  $(B_9C_3)$  icosahedra, with the hypothetical  $(B_9C_3)CBC$  configuration limiting the range of stable boron carbide compounds at 33 at.% C.<sup>25,46</sup> However, the latter finding is in contradiction with an established concept

that due to the internal bonding constraints, the maximum number of carbon atoms that can substitute boron in the icosahedra is two.<sup>67</sup> Following this concept and assuming  $(B_{10}C_2)CBC$  as the most carbon-rich configuration of boron carbide, the theoretical limit for the carbon-rich edge of the homogeneity range should not exceed 25 at.% C.

There is a lack of agreement in the scientific community on the nature of the structural changes in boron carbide at decreasing carbon concentrations. While it is generally accepted that the carbon atoms substitute boron atoms in the rhombohedral lattice, different views exist on whether the chain or the icosahedral atoms are preferentially substituted. Based on entropic and energetic considerations, Emin conjectured that preferred substitution occurs in the chain sites.<sup>36</sup> According to this theory, the number of CBB chains in the structure will increase until all material is comprised of the  $(B_{11}C)CBB$  units, which corresponds to the  $B_{6.5}C$  stoichiometry at 13.3 at.% C. For lower carbon concentrations, the substitution will take place within the icosahedra, rendering the idealized  $(B_{12})CBB$  configuration for the most boron-rich  $B_{14}C$  stoichiometry at 6.7 at.% C. This model provides basis for a consistent interpretation of the observed trends in the compositional dependence of electrical and thermal transport properties,<sup>68–74</sup> elastic properties,<sup>75</sup> structural data,<sup>33</sup> and vibrational frequencies and intensities incurred from Raman and infrared (IR) measurements.<sup>53,58,59,76</sup>

An alternative interpretation of the available X-ray diffraction (XRD) data maintains that carbon is preferably replaced by boron in the icosahedral sites.<sup>32,77,78</sup> In this model, the number of  $(B_{12})$  icosahedra in the material increases as the composition approaches 13 at.% C from the carbon-rich end; the structural configuration for the stoichiometric  $B_{6.5}C$  phase is given as  $(B_{12})CBC$ ; and the substitution of boron into the chain sites occupied by carbon occurs in the 8–13 at.% C range of compositions. This view is also supported by the DFT calculations, which consistently indicate that the  $(B_{12})CBC$  configuration is more stable than the  $(B_{11}C)CBB$  one, both from the energy minimization considerations and from a better correlation with the experimental lattice parameters.<sup>4,38,40,43</sup>

Comparative DFT calculations of the free energy and the structural parameters of various possible configurations of chain and icosahedral units for different boron carbide stoichiometries have been reported by several authors.<sup>4,40,43</sup> Fanchini *et al.*<sup>40</sup> observed that the calculated free energies for a number of different atomic configurations, referred to as *polytypes*, fall into a small disorder potential of  $\Delta V \approx 0.2$  eV (Fig. 4), corresponding to typical temperature variations encountered during boron carbide synthesis.<sup>3</sup> Based on this consideration, Fanchini and co-workers proposed that various boron carbide polytypes with energy differences smaller than the disorder potential can coexist at any given boron carbide composition.<sup>40</sup>

In practice, the structure of as synthesized boron carbide is more disordered than indicated by the idealized models presented above. Theoretical calculations predict  $(B_{12})B\Box C$  ( $\square$  for vacancy) to be the most stable configuration at the boron-rich end of the homogeneity range.<sup>43</sup> Refinement of the XRD data for  $B_{9.5}C$  implies that at this composition, up to 25% of CBC chains are statistically replaced by the 4-atom  $B_B^{BB}$  units, where the two central atoms of the unit lie near a plane normal to the threefold axis, bonding to the two terminal unit atoms and to the three icosahedral atoms.<sup>52</sup> Neutron diffraction observations give evidence of the presence of non-linear chains with a displaced central atom, as well as chains with a vacancy in the central chain site, along with the regular CBC and (possibly) CBB chains and icosahedral units in the more boron-rich compositions.<sup>11,34</sup> Interpretation of the IR absorption spectra and analysis of the resulting phonon oscillator strengths indicate statistical distribution of several structural elements, e.g.,  $(B_{12})$  and  $(B_{11}C)$  icosahedra, CBC and CBB chains, as well as chainless units, at all compositions within the homogeneity range, as illustrated in Fig. 5.<sup>54</sup> However, it should be noted that the results of such calculation are

contingent upon the specific assumptions made during the derivation of the model, and other variations of the compositional dependencies of the structural elements that form boron carbide have also been reported.<sup>55,79</sup>

The presence of defects is essential for boron carbides. As shown by Balakrishnarajan *et al.*,<sup>42</sup> disorders in the atomic arrangement are a part of the ground-state properties of boron carbide, and are not due to entropic effects at high temperatures. This is not unique for boron carbide, but rather a common property of boron-rich solids. In  $\beta$ -rhombohedral boron, for example, the presence of intrinsic defects has been shown to result in macroscopic residual entropy, suggesting that  $\beta$ -boron could be characterized as a frustrated system.<sup>80</sup> The case of boron carbide may be on line with this research.

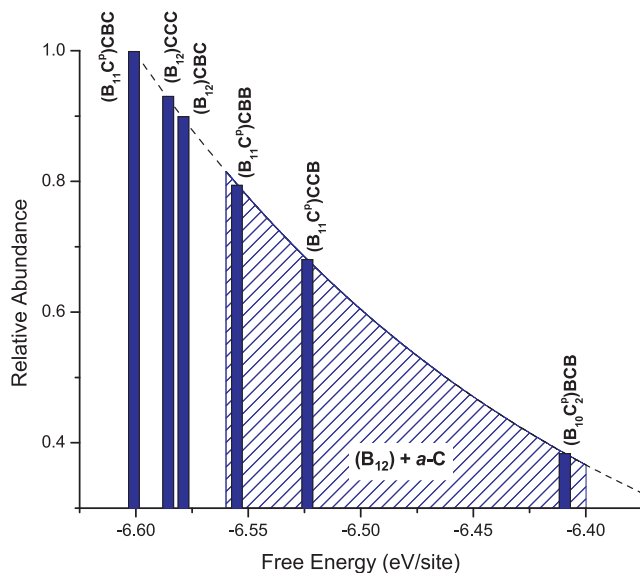


**Fig. 4.** Gibbs energies ( $G_i$ ) and the relative abundances  $f_i \propto \exp(-G_i/\Delta V)$  of selected boron carbide polytypes corresponding to the disorder potential of  $\Delta V = 0.2$  eV (dash line), after Fanchini *et al.*<sup>40</sup> Stability range for a segregated boron-amorphous carbon ( $B_{12}$ ) +  $a\text{-C}$  phase is also shown.

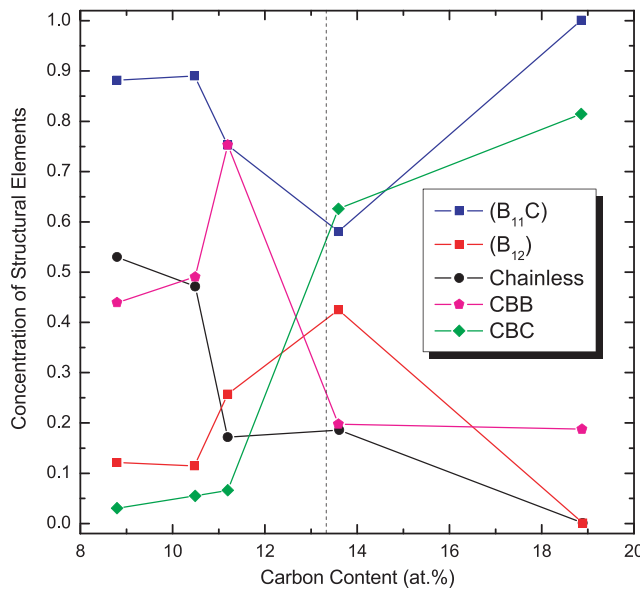


**Fig. 5.** Distribution of chain and icosahedral structural units across the homogeneity range in boron carbide obtained from the analysis of IR absorption data by Werheit and co-workers. Reproduced from Kuhlmann *et al.*,<sup>54</sup> with permission; ©1992 Elsevier.

Finally, a crucial issue that structural experimental and theoretical data do not take into account is the presence of free carbon in as-synthesized boron carbide. That is, all polycrystalline boron carbides contain impurities in the form of free carbon that can exist as either amorphous carbon or intra-granular graphitic inclusions, as shown by a systematic characterization of hot-pressed boron carbide ceramics by Chen *et al.*<sup>81</sup>

## II. Electronic Structure, Electronic and Optical Properties

Early work by Lagrenaudie established that boron carbide was a *p*-type semiconductor with an estimated band gap of 1.64 eV.<sup>82</sup> This is much smaller than the band gap of other semiconductor ceramics, e.g.,  $E_g \sim 3$  eV as in silicon carbide. Other estimations for the band gap of boron carbide have also been reported. Werheit *et al.* measured an indirect gap of 0.48 eV<sup>83</sup> by optical measurements; the same group reported in a later work a band gap of 2.09 eV, suggesting that a wide range of gaps could be identified in the boron carbide structure within the stoichiometric range of  $B_{4.3}C-B_{11}C$ .<sup>84</sup> Larger band gaps, typically exceeding 3 eV, are consistently obtained in theoretical band structure calculations, suggesting that the models do not adequately account for the disorder in the material which could give rise to midgap states.<sup>35,37,38,64,85,86</sup> Examples of the calculated electronic density of states (DOS) showing estimated band gaps for the  $(B_{12})CCC$ <sup>86</sup> and the  $(B_{12})CBC$ <sup>85</sup> atomic configurations are given in Fig. 6. One important observation is that the presence of an intermediate gap state in  $(B_{12})CCC$ , according to calculations by Dekura *et al.*,<sup>86</sup> results in a smaller band gap of only 1.56 eV in this structure. In the case of  $(B_{12})CBC$ , Calandra *et al.* report that 88% of total DOS at the Fermi level arise from the icosahedra; in particular, boron atoms in polar positions give the largest contribution to the conduction processes.<sup>85</sup>

Electronic band structure calculations confirm the semiconducting nature of boron carbide for the stoichiometric  $B_4C$

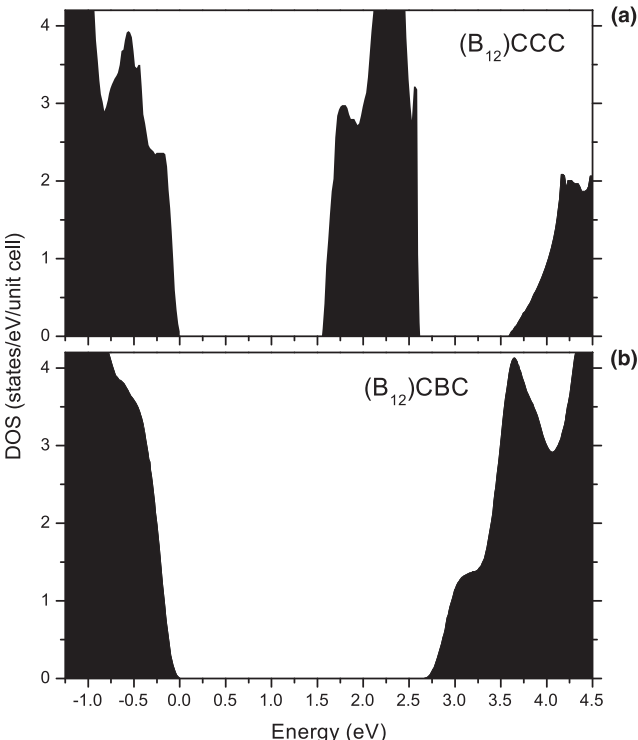


**Fig. 6.** Calculated electronic DOS for (a)  $(B_{12})CCC$ <sup>86</sup> and (b)  $(B_{12})CBC$ <sup>85</sup> polytypes of boron carbide. An intermediate gap state is formed in  $(B_{12})CCC$ . The top of the valence band is taken as the energy origin. The Fermi level is located at zero for  $(B_{12})CCC$  while it is at -0.52 eV for  $(B_{12})CBC$ .

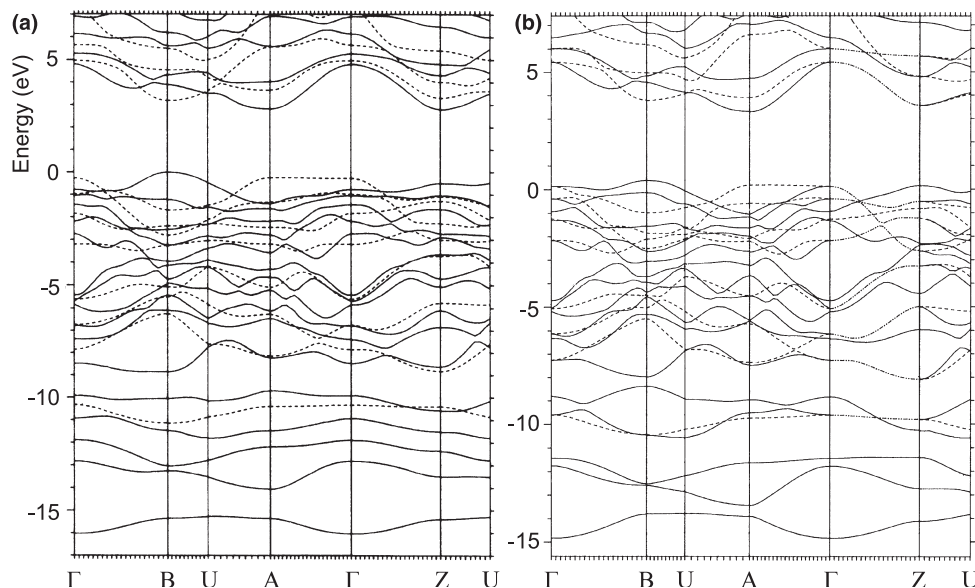


**Fig. 7.** Calculated energy bands for (a) the  $(\text{B}_{11}\text{C})\text{CBC}$  and (b) the  $(\text{B}_{12})\text{CBC}$  polytypes of boron carbide. The solid and the dash bands represent states that are, respectively, even and odd under reflection in a vertical plane. Zero energy corresponds to Fermi level. Reproduced from Kleinman,<sup>87</sup> with permission; ©1991 American Institute of Physics.

with 48 valence electrons.<sup>35,37,86</sup> However, more boron-rich compounds, characterized by valence electron deficiencies are consistently found to be metallic.<sup>35,38,85</sup> This is a direct consequence of the band theory stating that a crystal with odd number of valence electrons must be a metal, independent of the calculation method.<sup>5</sup> Figure 7 shows electronic band structures calculated by Kleinman's group for the  $(\text{B}_{11}\text{C})\text{CBC}$  and the  $(\text{B}_{12})\text{CBC}$  configurations.<sup>37,38,87</sup> As follows from an examination of Fig. 7, the main difference between the two structures is the position of the Fermi level, which indicates the semiconducting nature of  $(\text{B}_{11}\text{C})\text{CBC}$  and the metallic nature of  $(\text{B}_{12})\text{CBC}$ . For the  $(\text{B}_{12})\text{CCC}$  configuration, as illustrated in Fig. 6, a distinct feature of the band structure is the presence of the gap state of nonbonding character, predominantly arising from the  $p$  orbital of the central C atom in the chain.<sup>86</sup> This may explain the origins for  $\text{B}_4\text{C}$  refusal of assuming the  $(\text{B}_{12})\text{CCC}$  atomic configuration.

Experimentally, boron carbide was found to be a semiconductor throughout the entire homogeneity range, with its electronic properties dominated by the hopping-type transport.<sup>68,88,89</sup> The direct current (dc) conductivity of boron carbide as a function of carbon content, as measured by several groups,<sup>68,89–92</sup> is presented in Fig. 8. Qualitatively, the maximum in conductivity occurs at ~13 at.% C, corresponding to the  $\text{B}_{6.5}\text{C}$  stoichiometry. This observation, as well as similar trends in the compositional dependences of other boron carbide properties (e.g., structural parameters, see Fig. 3), have been attributed to different mechanisms for boron substitutions into the lattice sites occupied by carbon atoms, as discussed in Section I. Several related models have been also proposed in the literature for explaining boron carbide transport properties.

Emin advanced a charge transport model based on the small bipolaron hopping mechanism.<sup>93–96</sup> In this model, the charge carriers in boron carbide are pairs of holes that move by a succession of thermally activated phonon-assisted hops between electronic states on inequivalent  $\text{B}_{11}\text{C}$  icosahedra. The pairing of the holes on  $\text{B}_{11}\text{C}$  icosahedra is viewed as a result of the disproportionation reaction,  $2(\text{B}_{11}\text{C})^0 \rightarrow (\text{B}_{11}\text{C})^- + (\text{B}_{11}\text{C})^+$ , resulting in the formation of an electron-deficient  $(\text{B}_{11}\text{C})^+$  icosahedron, which is a chemical equivalent of a bipolaron. This theory, together with an associated structural model<sup>36</sup> (Section I), was able to interpret the observed compositional, temperature and pressure dependence of boron carbide conductivity, as well as the variations

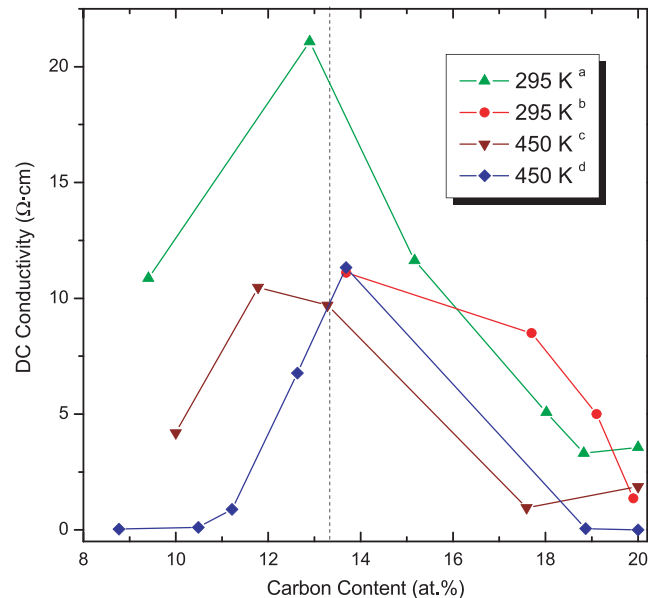


**Fig. 8.** Compositional dependence of dc conductivity in boron carbide at different temperatures. Data from (a) Samara *et al.*<sup>92</sup>; (b) Werheit *et al.*<sup>90,91</sup>; (c) Wood *et al.*<sup>68</sup>; (d) Schmechel *et al.*<sup>89</sup>

in Hall mobility, Seebeck coefficient, dielectric constants, and magnetic susceptibility of boron carbide with temperature and carbon concentration.<sup>68,72,74,92,97,98</sup>

However, it is important to note that the apparent correlation of the experimental data with the Emin's transport model is contingent upon several factors. Crucial for the interpretation of the compositional dependencies of physical properties (e.g., electrical conductivity, Fig. 8) in terms of small bipolaron hopping is Emin's conjecture that the structure of the  $\text{B}_{6.5}\text{C}$  compound is described by the  $(\text{B}_{11}\text{C})\text{CBB}$  atomic configuration, providing sufficient concentrations of the  $(\text{B}_{11}\text{C})$  units required for the formation of bipolarons at this stoichiometry. However, as discussed in Section I, there is no direct empirical evidence in support of this structural model. Moreover, both the refinement of XRD data and the results of *all* available theoretical *ab initio* calculations support an alternative structural model, which predicts gradual substitution of the icosahedral carbon atoms with boron

as the carbon concentration changes from 20 at.% to 13.3 at.%. In this model, the preferred atomic configuration for the  $B_{6.5}C$  compound is given by the  $(B_{12})CBC$  formula, providing very limited availability of the  $(B_{11}C)$  units, which is exactly opposite to the requirements of Emin's theory. Other inconsistencies of the small bipolaron hopping model for boron carbide, such as an overestimate of carrier concentrations and the evidence for multiple activation energies in the temperature dependence of electric conductivity, have also been discussed in the literature.<sup>99</sup>

An alternative interpretation of boron carbide transport properties has been proposed by Werheit and co-workers.<sup>79,89,100,101</sup> They suggest that the semiconducting nature of boron carbide arises from the structural disorder throughout the entire homogeneity range. The intrinsic defects associated with disorder are proposed to be Jahn-Teller distortion of the icosahedra,<sup>100</sup> missing or incomplete occupation of specific atomic sites, statistical occupation of equivalent sites, or anti-site defects.<sup>54,55,79</sup> Werheit maintains that the defects in boron carbide generate split-off valence states in the band gap, which exactly compensate electron deficiency of the idealized structures (e.g.,  $(B_{12})CBC$ ) that are theoretically found to be metallic. According to Werheit,<sup>101</sup> high concentration of gap states near the valence band is responsible for the low *p*-type electrical conductivity in boron carbide. In addition to the electrical conductivity in extended band states, hopping-type conduction in localized gap states is predicted by this model. The compositional dependencies of physical properties in boron carbide, such as electrical conductivity shown in Fig. 8, can then be correlated with the total concentration of intrinsic defects, such as the one illustrated in Fig. 5. However, this model suffers from the lack of independent verification. The distribution of structural elements, as proposed by Werheit and co-workers,<sup>54,55,79</sup> relies entirely on the interpretation of specific bands in the IR absorption spectra of boron carbide obtained by the same group. It will be discussed in Section III that alternative interpretations offered in the literature of the IR data provide alternative explanations to Werheit's analysis. In addition, their model requires a pre-selection of structural elements that Werheit and co-workers limit to  $(B_{12})$  and  $(B_{11}C)$  icosahedra and CBC, CBB, and  $B\Box B$  chains. As discussed in Section I, while neutron diffraction data give evidence for vacancies in the central chain site, other possible atomic configurations, such as the  $(B_{10}C_2)$  icosahedra, the  $C\Box B$  chains, the nonlinear chains, the 4-atomic boron units replacing the chains, *etc.*, may also be present in boron carbide at varying stoichiometries. Accounting for these additional structural elements would inevitably alter Werheit's compositional distribution curves, such as the one shown in Fig. 5.

The origin of disorder in boron carbide has been investigated using quantum chemical methods by Balakrishnarajan *et al.*,<sup>42</sup> who analyzed the nature of the molecular orbitals corresponding to the  $(B_{12})$  icosahedra and CBC chains and interactions among them in the most symmetric  $(B_{12})CBC$  structure. They also studied the effect on the bonding of adding or removing an electron from the unit cell. The calculations have shown that the addition of electrons expands the unit cell, elongating and weakening all bonds. In particular, the carbon atoms tend to change hybridization from  $sp^2$  to  $sp^3$  as the total molecular charge is increased. This group also studied the changes in the bonding nature with the varying carbon content, concluding that partial substitution of carbon by boron atoms creates inevitable disorder because it is energetically and entropically favored. In particular, calculations indicate that disorder is localized at the carbon sites and the bonding of B/C covalent network in defective boron carbide is stronger than in the stoichiometric electron-precise  $B_4C$ .<sup>42</sup> The localization of the electronic states arising from the B/C disorder therefore leads to semiconducting nature of boron carbide throughout its entire compositional range.

**Table I. Optical Constants of Hot-Pressed Boron Carbide<sup>102</sup>**

Wavelength (nm)	<i>n</i> (a.u.)	<i>k</i> (a.u.)
49.0	0.5	0.41
54.3	0.45	0.63
58.0	0.45	0.74
67.2	0.53	1.02
74.0	0.60	1.15
83.5	0.77	1.45
92.0	0.86	1.61
104.8	1.11	1.81
121.6	1.77	2.05

The electronic states discussed above determine the optical properties of boron carbide and therefore can be probed using optical techniques. Optical constants of hot-pressed boron carbide with a presumed  $B_4C$  stoichiometry, calculated by Larraquet *et al.* via reflectance measurements in the extreme ultraviolet spectral region are listed in Table I.<sup>102</sup> Werheit *et al.* measured dielectric functions of boron carbide samples with varying history and stoichiometry, as illustrated in Fig. 9.<sup>103</sup> A number of critical points for interband transitions identified from the data in Fig. 9 indicate that the band gap of boron carbide does not exceed 2.5 eV. This work also demonstrated that the imaginary part of the dielectric function reached maximum near ~13 at.% C, which was correlated by the authors to the highest structural disorder in boron carbide at the  $B_{6.5}C$  stoichiometry.<sup>103</sup>

The absorption coefficients obtained from optical transmission measurements on  $B_{4.3}C$  samples with varying degrees of structural disorder<sup>104,105</sup> are shown in Fig. 10. Optical absorption in a single crystal ( $\alpha \approx 3000 \text{ cm}^{-1}$ ) is higher than that in polycrystalline samples; however, the correlation of  $\alpha$  with structural disorder cannot be unambiguously established because a more ordered polycrystalline sample obtained by hot isostatic pressing (HIP) shows lower absorption below the absorption edge than the less ordered commercial sample obtained by hot pressing (HP). The increase in absorption coefficient toward lower energies in the single crystal data has been attributed to charge carriers,<sup>105</sup> in correlation with both the hopping-type and the Drude-type transport. Werheit and co-workers have identified several indirect transitions between 0.47 and 3.58 eV via deconvolution of the absorption edge shown in Fig. 10.<sup>104,105</sup> They assign such processes to transitions between various electronic states within the band gap.

Feng *et al.* used nonresonant X-ray Raman scattering (XRS) technique along with site-specific *ab initio* calculations to detect substitutional disorder in carbon-rich boron carbide.<sup>62</sup> The results of this study show that boron preferentially occupies the chain center site generating a delocalized *p*-type exciton. Enlarged view of the near-edge region for the boron XRS spectrum of  $B_4C$  shown in Fig. 11 identifies the exciton related feature at ~1 eV. Werheit compared these XRS results with their optical absorption data (Fig. 10) and found good agreement between the two; he also proposed that the higher absorption of the single crystal boron carbide in the range of 1.0–1.5 eV (Fig. 10) must be due to smaller concentrations of extrinsic structural distortions resulting in higher probability of exciton generation compared to the polycrystalline material.<sup>84</sup>

Figure 12 shows the photoluminescence spectrum of a polycrystalline  $B_{4.23}C$  sample measured by Schmeichel *et al.* using the excitation energy of 2.4 eV.<sup>106</sup> The features at 1.56 and 1.5695 eV in the photoluminescence versus photon energy dependence have been attributed to the indirect recombination of free excitons in the center B atom in CBC and CBB chains, respectively.<sup>84</sup> Further, Werheit *et al.* reported photoluminescence measurements on a set of isotope-enriched boron carbide samples spanning the entire homogeneity range using an excitation energy of 1.165 eV.<sup>107</sup> They assigned the

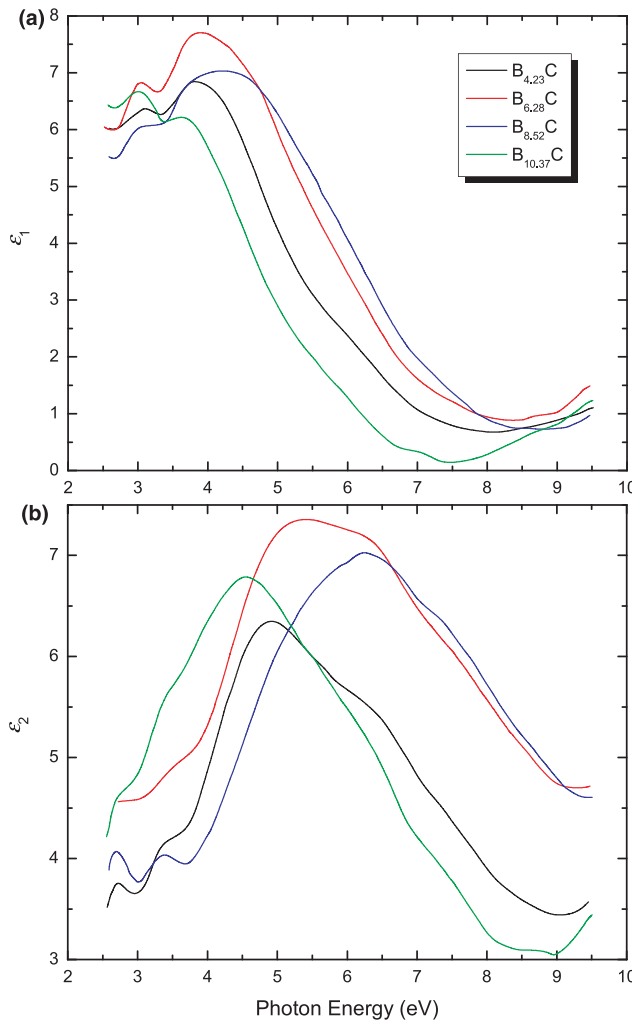


**Fig. 9.** (a) Real and (b) imaginary parts of the dielectric function of boron carbide with different stoichiometry. Reproduced from Werheit *et al.*,<sup>103</sup> with permission; ©1997 Elsevier.

various luminescence peaks to the presence of localized gap states and the resulting transitions between such states and the energy bands. Combining the optical absorption, photoluminescence, and charge transport data for electron transition energies, Werheit proposed an energy band schematic consisting of a 2.09 eV band gap, several disorder induced intermediate gap states extending 1.2 eV above the valence band edge, excitonic level at 1.56 eV above the valence band edge, and an electron trap level around 0.27 eV below the bottom of the conduction band, as shown in Fig. 13.<sup>84,107,108</sup>

### III. Lattice Dynamics and Vibrational Properties

For a boron carbide crystal of  $R\bar{3}m$  symmetry, group theory predicts the following representation for the normal modes of lattice dynamics:<sup>109</sup>

$$5A_{1g} + 2A_{1u} + 2A_{2g} + 6A_{2u} + 7E_g + 8E_u. \quad (1)$$

The 12 modes of  $A_{1g}$  and  $E_g$  symmetry are Raman active, the 14 modes of  $A_{2u}$  and  $E_u$  symmetry are IR active, and the  $A_{1u}$  and  $A_{2g}$  modes are optically inactive. By removing zero-frequency modes, the number of IR active modes becomes 12.<sup>109</sup> For boron carbide polytypes that deviate from true  $R\bar{3}m$  symmetry, e.g., when a carbon atom is introduced into the icosahedron, the above selection rules are not valid and a higher number of modes is expected in the experimental spectra.

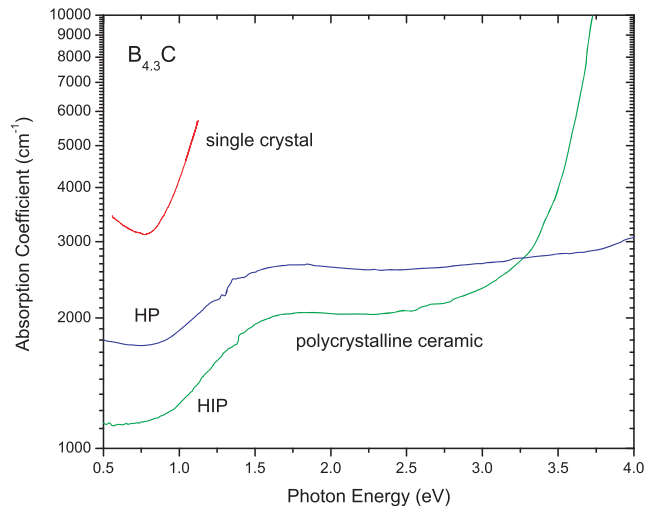


**Fig. 10.** Absorption coefficient versus photon energy measured on the (111) surface of a single crystal, on a high quality HIP polycrystalline sample, and on a commercial HP polycrystalline boron carbide ceramic. All samples are of the  $B_{4.3}C$  stoichiometry. Data from Werheit *et al.*<sup>104,105</sup>

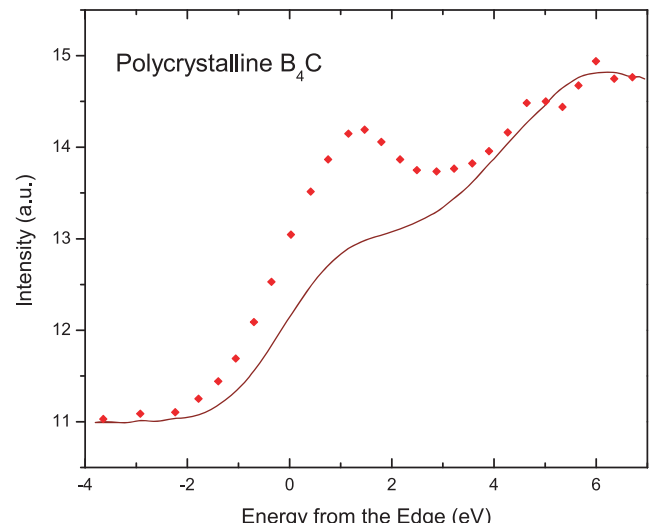


**Fig. 11.** Fragment of an XRS spectrum of polycrystalline boron carbide for a momentum transfer of  $1.05 \text{ \AA}^{-1}$  (dots) and the background of icosahedral B atoms (solid line) calculated for the  $(B_{12})CBC$  atomic arrangement. Data from Feng *et al.*<sup>62</sup>

The Raman and IR frequencies have been calculated for the  $(B_{12})CBC$  polytype from parametric fitting of the valence force constants,<sup>109,110</sup> and for the  $(B_{12})CBC$ ,  $(B_{12})CCC$ ,  $(B_{11}C^P)CBC$ , and  $(B_{11}C^C)CBC$  polytypes from *ab initio* DFT/DFPT calculations.<sup>65,111</sup> In Figs. 14 and 15, theoretical predictions for the IR and Raman active modes in the  $(B_{12})CBC$  and  $(B_{11}C^P)CBC$  polytypes are compared with the experimental spectra for boron carbide of matching stoichiometries, i.e.,  $B_{6.5}C$  and  $B_4C$ , respectively. It is immediately recognized that the use of simplified models for the evaluation of the force constants<sup>109</sup> do not yield reliable frequencies. Indeed, unambiguous identification of specific IR and Raman bands is impractical in this case [Figs. 14(a) and 15(a)]. On the other hand, for mode frequencies calculated by *ab initio* pseudopotential modeling by Lazzari *et al.*<sup>65</sup>, correlation with experiment is very good [Figs. 14(b) and 15(b)]. In this work, not only frequencies but also relative peak intensities have been correctly predicted in the calculated IR absorption spectrum of  $(B_{11}C^P)CBC$ , by accounting for the experimental mixing of

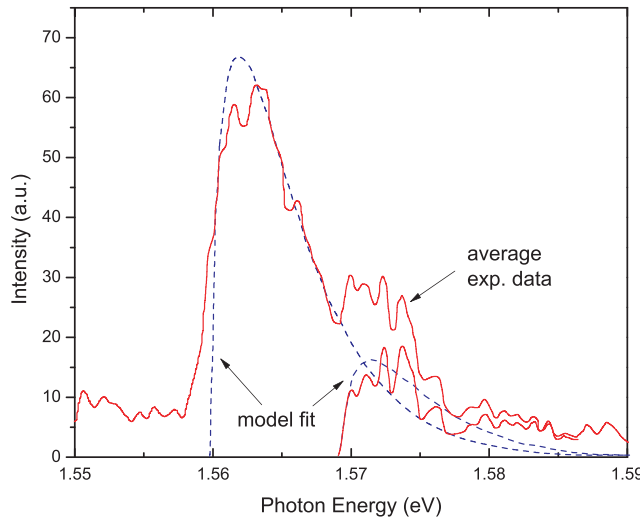


**Fig. 12.** Photoluminescence spectrum of polycrystalline boron carbide acquired at the excitation energy of 2.4 eV.<sup>106</sup> Squares, experimental results; dash lines, recombination models of free excitons:  $I(E) = \sqrt{E - E_0} \exp[(E - E_0)/k_B T_e]$ , with  $E_0 = 1.56$  eV (1.5695 eV) and the exciton temperature  $T_e = 46$  K; solid lines, averaged experimental results, before and after subtracting the 1.56 eV model fit. Reproduced from Werheit,<sup>84</sup> with permission; ©2006 Institute of Physics.

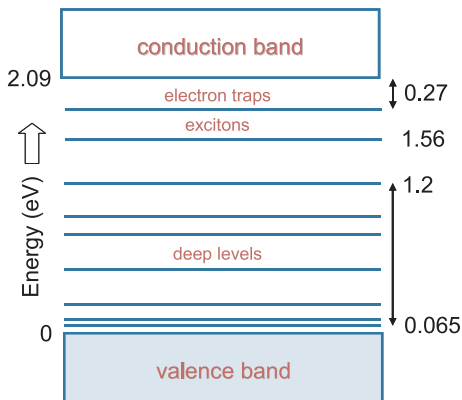


**Fig. 13.** Schematic of the structure of gap states in boron carbide developed by Werheit.<sup>84,107,108</sup>

polarizations for the  $A_{2u}$  and  $E_u$  modes.<sup>65</sup> Surprisingly, another *ab initio* study performed by Shirai *et al.*,<sup>111</sup> based on the same selection of pseudopotentials, yielded IR active modes that did not correlate well with the experiment (Fig. 14). Nevertheless, the latter work did elucidate an important observation that the IR modes shift to lower frequencies when a carbon atom is substituted by a boron atom in the icosahedra due to shortening of bond lengths.

There have been some efforts to correlate the specific IR and Raman modes to the atomic structure of boron carbide. According to Vast *et al.*,<sup>39</sup> the IR active  $E_u$  mode at  $396\text{ cm}^{-1}$  originates from the torsion of the CBC chain; the Raman active  $E_g$  mode at  $480\text{ cm}^{-1}$  arises from chain rotation perpendicular to the (111) plane; and the Raman active  $E_g$  mode at  $535\text{ cm}^{-1}$  is due to the libration of the  $(\text{B}_{11}\text{C})$  icosahedron. The atomic displacements from lattice dynamics calculated by Shirai *et al.*<sup>112</sup> are commonly referenced by experimentalists for peak assignments. Shirai's model predicts a Raman active  $A_{1g}$  mode at  $1080\text{ cm}^{-1}$  originating from the breathing vibrations of the  $(\text{B}_{12})$  icosahedron; an IR active  $E_u$  mode at  $1040\text{ cm}^{-1}$  resulting from complex atomic displacements due to chain bending, and antisymmetric stretching of an icosahedron; an IR active  $E_u$  mode at  $487\text{ cm}^{-1}$

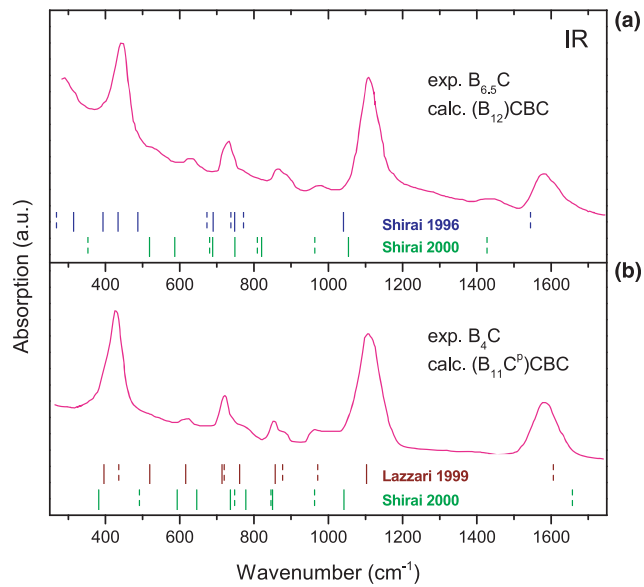


**Fig. 14.** Comparison of experimental and theoretical infrared absorption spectra of boron carbide: (a) FTIR on hot-pressed  $\text{B}_{6.5}\text{C}^{55}$  versus parameterized valence force model<sup>109</sup> and *ab initio* calculation<sup>111</sup> for  $(\text{B}_{12})$  CBC; (b) FTIR on hot pressed  $\text{B}_{4.3}\text{C}^{55}$  versus *ab initio* calculation for  $(\text{B}_{11}\text{C}^{\text{P}})\text{CBC}$ .<sup>65,111</sup> Solid lines:  $E_u$  modes; dash lines:  $A_{2u}$  modes.

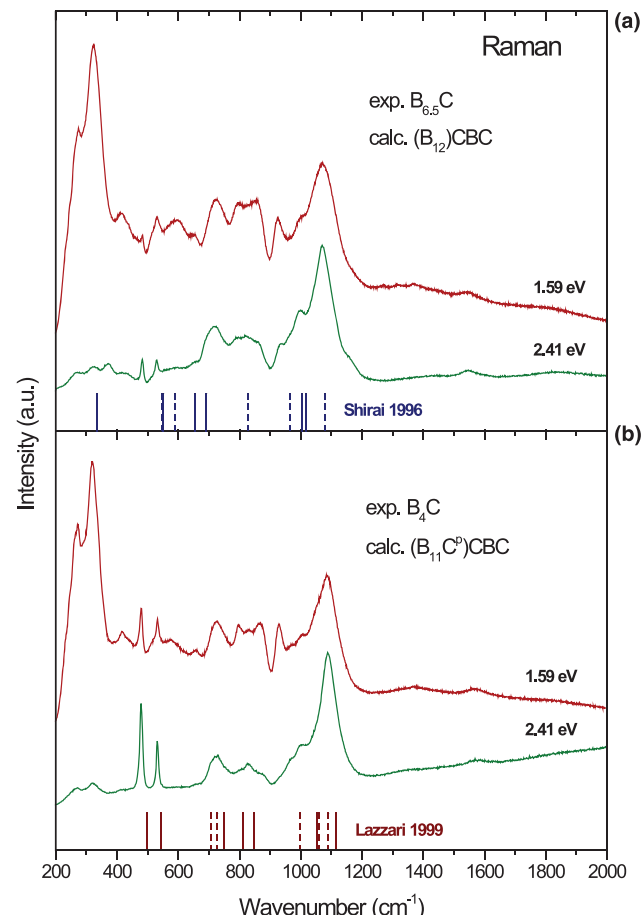


**Fig. 15.** Comparison of experimental and theoretical Raman spectra of boron carbide: (a) dispersive Raman (laser excitations 1.59 and 2.41 eV) on hot-pressed  $\text{B}_{6.5}\text{C}$  (this work) versus parameterized valence force model for  $(\text{B}_{12})\text{CBC}$ ;<sup>109</sup> (b) dispersive Raman (1.59 eV; 2.41 eV) on hot-pressed  $\text{B}_4\text{C}$  (this work) versus *ab initio* calculation for  $(\text{B}_{11}\text{C}^{\text{P}})\text{CBC}$ .<sup>65</sup> Solid lines:  $E_g$  modes; dash lines:  $A_{1g}$  modes.

originating from chain bending; a Raman active  $E_g$  mode at  $335\text{ cm}^{-1}$  resulting from atomic displacements due to chain rotation and wagging of an icosahedron; and a Raman active  $E_g$  mode at  $172\text{ cm}^{-1}$  originating from rotation of an icosahedron. Both the parametric fitting model of Shirai *et al.* and the results of *ab initio* calculations by Vast and co-workers agree in assigning an IR active  $A_{2u}$  mode at  $\sim 1600\text{ cm}^{-1}$  to the antisymmetric stretching of the CBC chain.<sup>4,112</sup>

Vast and co-workers have also reported theoretical estimations for phonon density of states (PDOS) of the  $(\text{B}_{12})\text{CBC}$  compound.<sup>85</sup> According to this work, the icosahedral modes are responsible for most of the contribution to total PDOS at frequencies below  $1130\text{ cm}^{-1}$ , with the exception of the features between  $200$  and  $450\text{ cm}^{-1}$ , where notable contribution from the chain modes involving vibrations of boron atoms is observed, and the feature at  $1040\text{ cm}^{-1}$ , which has a significant contribution to PDOS from the vibrations of carbon atoms in the chain (Fig. 16). Also, this model predicts that the high frequency feature at  $1555\text{ cm}^{-1}$  arises from the chain modes that involve vibrations of both boron and carbon atoms.<sup>85</sup>

### (1) Infrared Spectroscopy Observations

The infrared spectra of boron carbide have been studied extensively by the group of Werheit<sup>54–56,105,113</sup> Typical FTIR data of absorption index,  $k$ , are shown in Fig. 14 for two boron carbide stoichiometries associated with different structural configurations: the carbon-rich  $\text{B}_{4.3}\text{C}$  compound and the intermediate  $\text{B}_{6.5}\text{C}$  compound. Werheit *et al.* attribute the observed band at  $\sim 1600\text{ cm}^{-1}$  to CBC chain stretching, the band at  $410\text{ cm}^{-1}$  to CBC chain bending, and all the remaining bands to intra-icosahedral vibrations in boron carbide.<sup>54,113</sup> Further, this group has interpreted the appearance

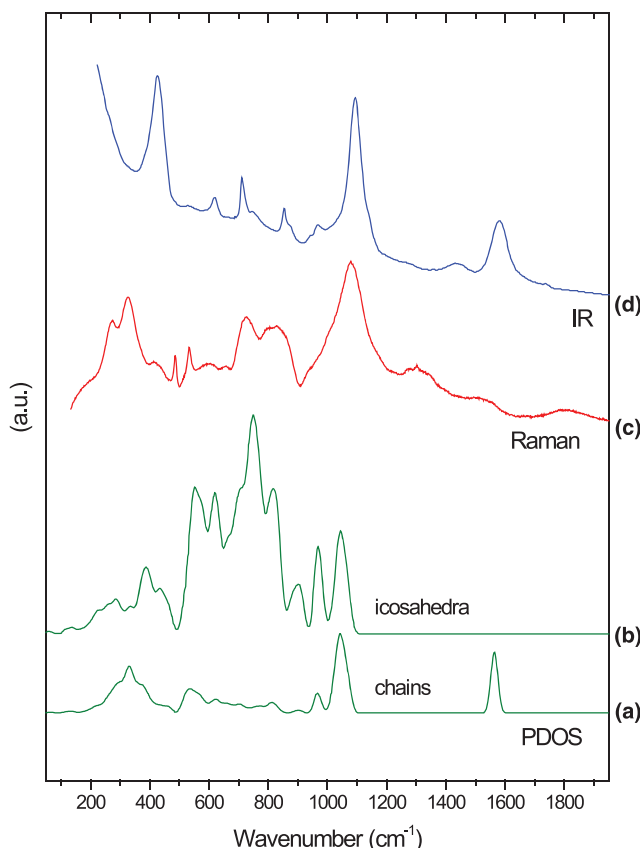


**Fig. 16.** Contribution from (a) chain modes and (b) icosahedral modes to PDOS calculated for the  $(\text{B}_{12})\text{CBC}$  polytype.<sup>85</sup> Experimental (c) Raman spectra (hot-pressed sample; laser energy  $1.96\text{ eV}$ ) and (d) FTIR absorption spectra<sup>56</sup> of the  $\text{B}_{6.5}\text{C}$  compound are shown for reference.

of bands at  $380$  and  $1450\text{ cm}^{-1}$  in more boron-rich compositions (Figs. 14 and 17) as new modes originating from stretching and bending of the chains that contain a C atom in the central site, such as the BCB or the CCC chains.<sup>55</sup>

The effect of isotope substitutions on the frequencies of IR active modes in boron carbide has also been investigated.<sup>30,53,55,56</sup> The isotope-dependent frequency shifts of IR modes in boron carbide composed of  $^{10}\text{B}_{4.3}^{12}\text{C}$  at the  $\text{B}_{4.3}\text{C}$  stoichiometry are shown in Fig. 18. The large frequency shift of the  $\sim 1600\text{ cm}^{-1}$  IR absorption band with both  $^{10}\text{B}$  and  $^{13}\text{C}$  isotopic substitutions imply substantial involvement of both B and C in this mode, which, combined with high frequency, indicates stiff bonding between boron and carbon atoms. Further, Aselage *et al.* challenged assignment of this band to stretching of the chain C–B bond, arguing that such a strong bond should form between boron and carbon atoms in the polar sites of the neighboring icosahedra.<sup>59</sup> However, as shown by Calandra *et al.*,<sup>85</sup> high frequency chain modes that involve vibrations of both B and C atoms are predicted by *ab initio* calculations, which supports Werheit's assignment of the  $\sim 1600\text{ cm}^{-1}$  IR absorption band to the CBC chain stretching.

### (2) Raman Spectroscopy Observations

The Raman spectra of boron carbide are characterized by a series of bands extending from  $200$  to  $1200\text{ cm}^{-1}$ .<sup>58–61,114</sup> There are conflicting assignments of the observed Raman bands to vibrations of icosahedra and the 3-atom linear chains.<sup>4,39,57–61,109,115</sup> Analysis of this is further complicated by the observed intensity dependence of the low-frequency bands on the excitation wavelength (energy).<sup>114</sup> Typical Raman spectra of two surfaces of a  $\text{B}_{4.3}\text{C}$  single crystal as a function of laser energy are shown in Fig. 19.

The group of Tallant, Aselage, and Emin<sup>57–59</sup> studied isotope and carbon content dependencies of boron carbides using the  $514.5\text{ nm}$  ( $2.41\text{ eV}$ ) laser. They assigned the two narrow bands at  $480$  and  $535\text{ cm}^{-1}$  to the stretching vibrations in the soft CBC chains. The intensity of both bands

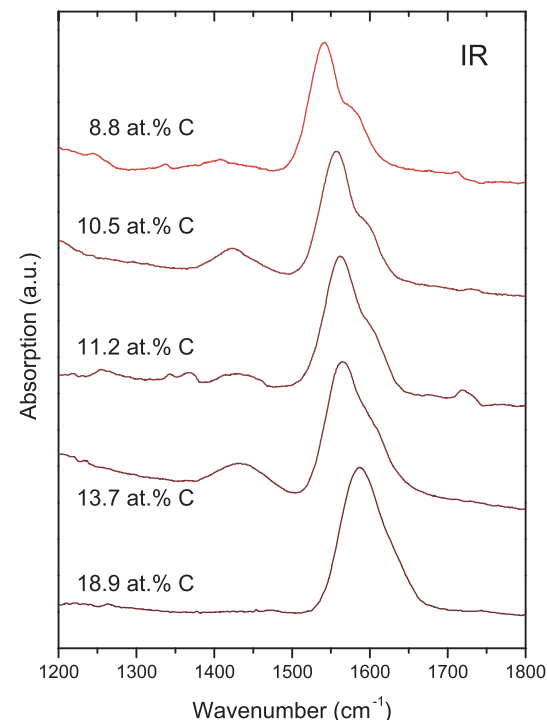


**Fig. 17.** Compositional dependence of the high frequency modes in the IR absorption spectra of boron carbide. Reproduced from Kuhlmann *et al.*,<sup>54</sup> with permission; ©1992 Elsevier.

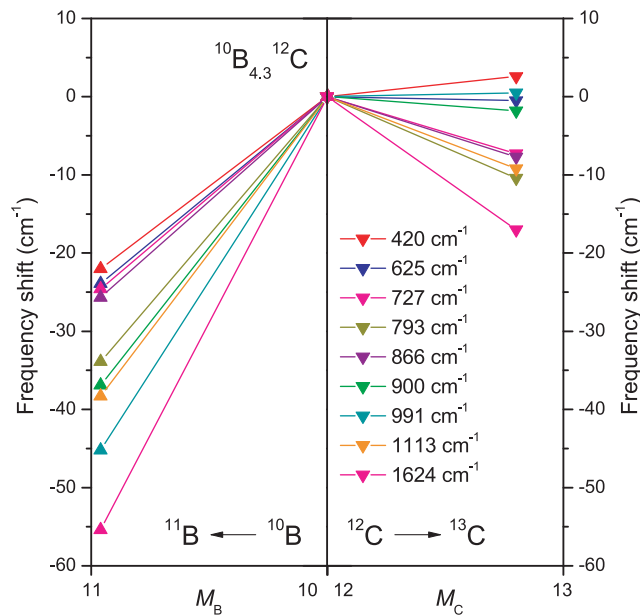


**Fig. 18.** Isotope-dependent frequency shift of the IR active modes in  $B_{4.3}C$  boron carbide, related to  $^{10}B_{4.3}^{12}C$ . Data from Werheit *et al.*<sup>56</sup>

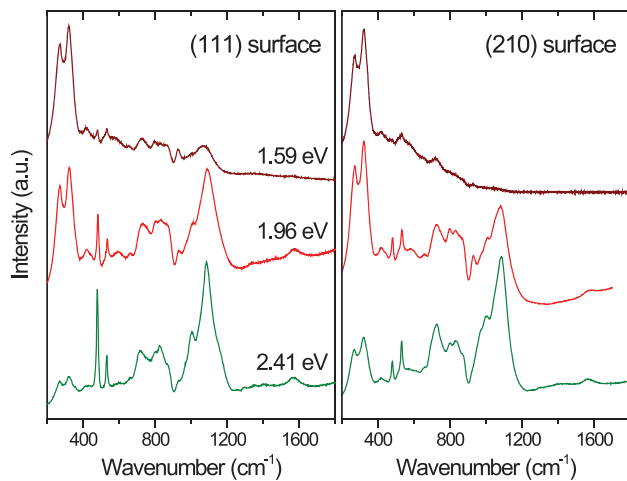


**Fig. 19.** Raman spectra of  $B_{4.3}C$  single crystal acquired at excitation wavelengths of 515 nm (2.41 eV), 633 nm (1.96 eV), and 780 nm (1.59 eV). Left panel: (111) surface. Reproduced from Domnich *et al.*,<sup>114</sup> with permission; ©2002 American Institute of Physics. Right panel: (210) surface (this work).

was found to diminish progressively with the decrease in carbon content, which was attributed to the gradual replacement of the CBC chains with the CBB chains. At the same time, the two bands at 270 and 320  $\text{cm}^{-1}$  were found to decrease in intensity with the decrease in carbon content, and a new narrow band at  $\sim 375 \text{ cm}^{-1}$  was found to appear and become more pronounced in the spectra of more boron-rich compounds. This latter feature was attributed to the appearance of the BBB chains at very low carbon concentrations. Further, according to this group,<sup>57–59</sup> the dependency of the high-frequency bands on carbon isotope and carbon concentration suggests that carbon atoms are present within icosahedra at all compositions.

The group of Werheit<sup>56,60,61,115,116</sup> studied isotopic and compositional dependencies of boron carbide using the 1070 nm (1.16 eV) laser. This group maintains that the spectra

acquired at higher laser energies are either coupled with the electronic states or are able to excite only surface phonons, due to the high absorption coefficient of boron carbide above the absorption edge,<sup>108,115</sup> which the Werheit group places at 3.5 eV.<sup>104</sup> At long excitation wavelength, the two bands at 270 and 320  $\text{cm}^{-1}$  become the primary features of the observed Raman spectra (Fig. 19). Following theoretical analysis of Shirai and Emura<sup>109</sup>, Werheit assigns these two bands to rotations of the CBC and CBB chains accompanied by wagging modes of the icosahedra. Werheit's group also finds that the intensities of the two bands at 270 and 320  $\text{cm}^{-1}$  diminish with the decrease in the carbon content, in agreement with the observations of Tallant, Aselage, and Emin.

According to *ab initio* DFT/DFTP calculations, no vibrational modes should be present in boron carbide at frequencies below 400  $\text{cm}^{-1}$ .<sup>39,65</sup> Vast and co-workers argued that the Raman bands observed in the experimental spectra at 270 and 320  $\text{cm}^{-1}$  arise from a lift in the selection rules induced by structural disorder and must reflect the DOS for acoustic phonons due to the  $\omega^4$  scaling law for scattering intensity at low frequencies.<sup>4</sup> However, this theory is in conflict with the following empirical observations: (i) the two bands at 270 and 320  $\text{cm}^{-1}$  are present in the anti-Stokes Raman spectra,<sup>108</sup> which reflects their true Raman nature; (ii) the intensity of the two bands at 270 and 320  $\text{cm}^{-1}$  increases with decreasing laser frequency (Fig. 19), which invalidates the  $\omega^4$  scaling law argument; and (iii) these bands are equally present in hot-pressed ceramics and in high purity single crystals (*cf.* Figs. 15 and 19), which questions their dependence on the structural defects and imperfections. Thus, the true nature of the bands at 270 and 320  $\text{cm}^{-1}$  in the Raman spectrum of boron carbide is still to be established.

The origin of the bands at 270 and 320  $\text{cm}^{-1}$  can be understood from the viewpoint of boron carbide being a frustrated system, as discussed in Section I. In a frustrated crystal, a perfectly ordered configuration with high symmetry is characterized by the formation of nonbonding states, as illustrated in Fig. 6. These nonbonding states can form the strong covalent bond by breaking the symmetry, at the cost of losing a covalent bond in another place. Formation of a strong local bond brings about an associated weak bond, and these weak bond or weak angle forces may be responsible for the appearance of low-frequency modes in the Raman spectra of boron carbide. The primitive-cell calculations (such as the ones by Lazzari *et al.*<sup>65</sup> and by Shirai *et al.*<sup>111</sup>), on the other hand, would completely eliminate such fluctuations over the crystal.

Assignment of the 480  $\text{cm}^{-1}$  band to chain rotation perpendicular to the (111) plane, implied by *ab initio* calculations of Lazzari *et al.*,<sup>65</sup> has been experimentally confirmed by the observations made on oriented boron carbide single crystals. As shown in Fig. 19, the intensity of the 480  $\text{cm}^{-1}$  band diminishes with respect to other Raman bands when the sample is rotated from the (111) orientation, when the scattering geometry is aligned with the 3-atom chain, to the (210) orientation, when the scattering geometry is at  $\sim 25^\circ$  angle to the 3-atom chain. This would be expected for a vibrational mode where maximum atomic displacements occur in directions perpendicular to the chain axis, such as the discussed CBC chain rotation mode.<sup>39</sup>

The Raman spectrum of boron carbide at higher frequencies (from 600 to 1200  $\text{cm}^{-1}$ ) is characterized by a number of broad bands that are believed to originate predominantly from the vibrations within the icosahedral units.<sup>39,58</sup> Following Shirai's mode assignments,<sup>112</sup> the major band at 1088  $\text{cm}^{-1}$  is referred to in some literature as the *icosahedral breathing mode*, or IBM. However, analysis of the Raman active modes for  $(B_{11}C)CBC$  [Fig. 15(a)] and the PDOS for  $(B_{12})CBC$  (Fig. 16), theoretically calculated by the Vast's group,<sup>65,85</sup> indicate that several modes originating from both the chains and the icosahedra may contribute to the broad feature around 1080  $\text{cm}^{-1}$ .

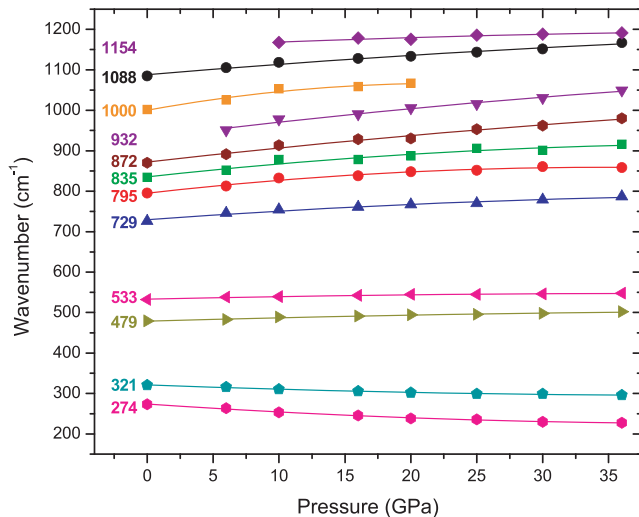


**Fig. 20.** Pressure dependence of band frequencies in the Raman spectra of single crystal B<sub>4</sub>C acquired at the laser energy of 2.41 eV. The best least-square fits are shown by solid lines. Analysis is based on the Raman spectra reported by Guo *et al.*<sup>119</sup>

Further insight into the nature of the Raman bands is provided by hydrostatic compression experiments reported by different groups.<sup>117–119</sup> Pressure dependence of band frequencies in the Raman spectra measured by Guo *et al.*,<sup>119</sup> up to 36 GPa are shown in Fig. 20. The phonon dispersion under pressure is described in terms of mode Grüneisen parameters  $\gamma_i$ , defined by

$$\gamma_i = -\frac{\partial \ln \omega_i}{\partial \ln V} = \frac{B_T}{\omega_i} \left( \frac{\partial \omega_i}{\partial P} \right), \quad (2)$$

where  $\omega_i$  is the mode phonon frequency,  $B_T$  is the isothermal bulk modulus,  $V$  is the volume, and  $P$  is the pressure. Second-order polynomial fitting of the data in Fig. 20 yields the values for  $\gamma_i$  listed in Table II.

The 1088 cm<sup>-1</sup> Raman band shows weak dependence on pressure ( $\gamma_{1088} = 0.59$ ), suggesting high stiffness of the associated vibrations. In view of the experimentally observed higher compressibility of icosahedra with respect to the unit cell,<sup>120</sup> this questions the assignment of the 1088 cm<sup>-1</sup> band to breathing vibrations of icosahedra, as proposed in some works.<sup>58,121</sup> The largest Grüneisen parameter of 1.38 is observed for the Raman band at 1000 cm<sup>-1</sup> (Table II). Taking into account the results of *ab initio* calculation by Lazzari *et al.*,<sup>65</sup> which predict a Raman active mode with the A<sub>1g</sub> symmetry (consistent with the icosahedron breathing) at 1000 cm<sup>-1</sup>, one might be tempted to identify this band as IBM. However, the 1000 cm<sup>-1</sup> band vanishes from the Raman spectra above 20 GPa (Fig. 20), whereas the icosahedra have been shown to be stable to at least 100 GPa under hydrostatic compression.<sup>120,122</sup> Splitting and sharpening of the high frequency bands becomes apparent at pressures in excess of 20 GPa;<sup>117–119</sup> the bands at 932 and 1154 cm<sup>-1</sup> become discernible in the Raman spectra only above 10 GPa (Fig. 20).

Selected band intensities with respect to the 1088 cm<sup>-1</sup> band are shown in Fig. 21, calculated using the Raman spectra acquired by Guo *et al.*<sup>119</sup> at laser excitation wavelengths of 515 nm (2.41 eV) and 633 nm (1.96 eV). The intensity of the 535 cm<sup>-1</sup> band decreases with pressure faster than the intensity of the 480 cm<sup>-1</sup> band, indicating different origins of these bands in accordance with Lazzari's calculations.<sup>65</sup> Of particular interest is the feature at 270 cm<sup>-1</sup>, which shows anomalous intensity dependence on pressure, peaking at ~25–30 GPa and falling off rapidly thereafter, a trend reminiscent of a resonance-type enhancement. However, this behavior is independent on laser excitation energy, which

**Table II.** Frequencies at Zero Pressure  $\omega_i$ , One-Phonon Quadratic Pressure Coefficients  $\frac{1}{2}(\frac{d^2\omega_i}{dP^2})$ , and Grüneisen Parameters  $\gamma_i$  for Raman Active Modes in the B<sub>4</sub>C Single Crystal

$\omega_i$ (cm <sup>-1</sup> )	$\frac{1}{2}(\frac{d^2\omega_i}{dP^2})$ (cm <sup>-1</sup> ·Pa <sup>-2</sup> )	$\gamma_i$
274	0.026	-1.90
321	0.015	-0.89
415	-0.001	0.26
479	-0.008	0.43
533	-0.010	0.33
729	-0.024	0.76
795	-0.054	1.09
836	-0.039	1.00
872	-0.021	0.99
932	-0.024	1.02
1000	-0.130	1.38
1088	-0.018	0.59
1154	-0.015	0.32

The values are obtained from best least-squares fits to measured pressure shifts of the Raman bands acquired at the laser energy of 2.41 eV by Guo *et al.*<sup>119</sup> The bulk modulus of B<sub>4</sub>C, required to compute  $\gamma_i$ , is taken from Manghnani *et al.*<sup>117</sup>

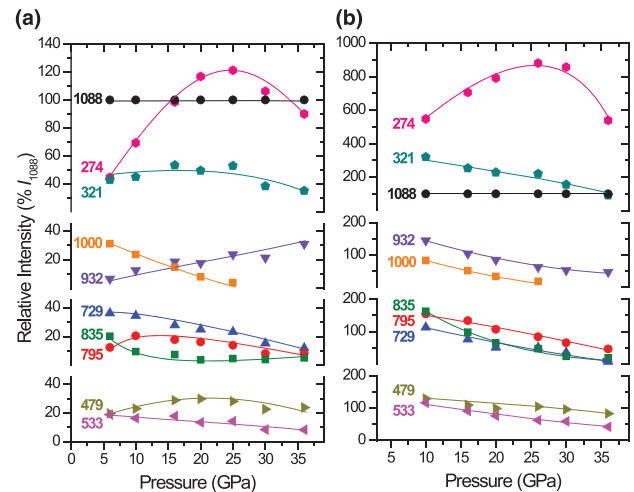


**Fig. 21.** Pressure dependence of band intensities in the Raman spectra of single crystal B<sub>4</sub>C acquired at the laser energy of (a) 2.41 eV and (b) 1.96 eV. Lines serve as guides to the eye. Analysis is based on the Raman spectra reported by Guo *et al.*<sup>119</sup>

questions possible assignment of this band to a resonance process. Another peculiarity of the two low-frequency bands at 270 and 320 cm<sup>-1</sup> is their negative pressure dispersion, as evidenced by their Grüneisen parameters of  $\gamma_{274} = -1.90$  and  $\gamma_{321} = -0.89$  (Table II). Pressure softening of zone-boundary acoustic phonons is a common feature of tetrahedral semiconductors that accounts for the negative thermal expansion coefficients usually found at low temperatures in these materials.<sup>123</sup> Soft acoustic phonons are also believed to induce shear instabilities leading to amorphization in quartz<sup>124,125</sup> and coesite.<sup>126</sup> However, ultrasonic measurements show that the Grüneisen parameters for the longitudinal and transverse acoustic modes in boron carbide are positive,  $\gamma_L = 1.21$  and  $\gamma_T = 0.33$ ,<sup>127</sup> which is in conflict with the assignment of the 270 and 320 cm<sup>-1</sup> bands to disorder-induced acoustic phonons as endorsed by Lazzari *et al.*<sup>65</sup>

Because amorphous/graphitic carbon inclusions are commonly present in commercial boron carbide, it is important to discuss the lattice dynamics properties associated with these forms of carbon. The nature of the Raman spectra of graphitic and amorphous carbon was investigated by Ferrari

*et al.*<sup>128</sup> A typical Raman spectrum of amorphous carbon is shown in Fig. 22. According to the literature, the graphite-like, also called tangential *G* band ( $1589\text{ cm}^{-1}$ ), derives from the in-plane stretching vibration of the double C=C bonds ( $sp^2$  carbon), and has the  $E_{2g}$  symmetry. In the ideal case of a large single crystal graphitic domain, the *G* band is the only one to appear. The disorder-induced *D* band ( $\approx 1300\text{--}1360\text{ cm}^{-1}$ ) is originating from the breathing vibrations of the sixfold aromatic rings in finite graphitic domains. The mechanism responsible for the appearance of the *D* band is the formation of an electron-hole pair caused by laser excitation and followed by one-phonon emission. It has been shown that the activation of the *D* band always requires an elastic defect-related scattering process;<sup>128</sup> the *D* band is indeed observed in  $sp^2$  bonded carbons containing vacancies, impurities or other symmetry-breaking defects. The *D* mode is of the  $A_{1g}$  symmetry and involves a phonon near the K zone boundary.

Tuinstra and Koenig noted that the ratio of the intensity of the *D* band with respect to the *G* band varies inversely with the size of the graphitic clusters.<sup>129</sup> This relation was later modified by Ferrari and Robertson to account for domains with increased electron confinement:<sup>128</sup>

$$\frac{I(D)}{I(G)} = \left( \frac{C(\lambda)}{L} \right) \quad L > 20\text{\AA} \quad \text{Tuinstra and Koenig}^{129} \quad (3)$$

$$\frac{I(D)}{I(G)} = \left( \frac{C(\lambda)}{L} \right)^{1/2} \quad L < 20\text{\AA} \quad \text{Ferrari and Robertson}^{128} \quad (4)$$

Here, constant  $C(\lambda)$  depends on the laser wavelength (e.g.,  $C(515\text{ nm}) = 40\text{ \AA}$ ), and  $L$  is the diameter of the  $sp^2$  domain.

The *G* band originating from carbon inclusions may be responsible for the occurrence of a feature at  $\sim 1580\text{ cm}^{-1}$  in the Raman spectra of boron carbide, as the ones shown in Fig. 15. Alternative explanation for the origin of this band has been offered by Werheit's group.<sup>60,116</sup> They argued that substitution of a boron atom for the end carbon atom in the CBC chain should lead to modified selection rules that would make stretching vibrations in the CBB chain Raman active. This is a valid assumption noting that the calculated frequency of the antisymmetric stretching mode in the CBC chain is placed around  $1600\text{ cm}^{-1}$  (Figs. 14 and 16), and the  $\sim 1580\text{ cm}^{-1}$  feature is commonly observed in the Raman spectra of high purity single crystal boron carbide samples that are presumably free of carbon inclusions (Fig. 19).

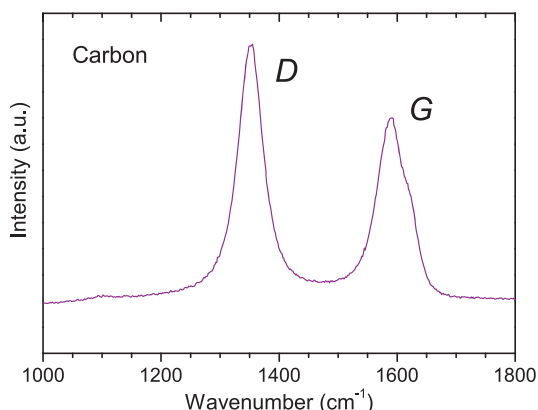


Fig. 22. Raman spectrum of amorphous/graphitic carbon with characteristic *D* and *G* bands.

#### IV. Atomic Bonding, Elastic and Mechanical Properties

Elastic and mechanical properties of boron carbide are derivative of such characteristics of atomic bonding as localization and delocalization, ionicity and covalence of the bonds and electron density in inter-atomic regions. In particular, higher stiffness and hardness is associated with more localized covalent bonds and higher inter-atomic electron density. Four types of atomic bonds can be identified for boron carbide in the  $R\bar{3}m$  symmetry (Fig. 1): (i) the *intrachain* bond, which connects the end atom and the center atom in the 3-atom chain and has a  $\pi$  character; (ii) the *chain-icosahedron* bond, which connects the end atom in the 3-atom chain to an atom in the equatorial site of the icosahedron; (iii) the *intericosahedral* bonds, which connect atoms in the polar sites of neighboring icosahedra and originate from  $sp$  hybridized orbitals; and (iv) the highly delocalized *intraicosahedral*  $sp^2$  bonds, which connect atoms within the icosahedron. Refinement of X-ray and neutron diffraction data shows that the intrachain bond has the shortest length at all stoichiometries; it is followed by the chain-icosahedron bond, the intericosahedral bond, and the intraicosahedral bonds.<sup>34,51,52,77,130</sup> For bonds of similar nature, the bond length is inversely related to the bond stiffness, which implies that the intrachain bonds are the most rigid ones and the intraicosahedral bonds are the most compliant ones in boron carbide. This finding is supported by the available theoretical calculations of bond strength/hardness for several possible configurations of boron and carbon atoms in the stoichiometric  $\text{B}_4\text{C}$  and  $\text{B}_{6.5}\text{C}$ .<sup>35,41,45,131</sup> The comparable magnitudes of the inter- and the intraicosahedral bond strengths were used as the basis for Emin's classification of boron carbide as *inverted molecular solid*, or a solid composed of strongly bound molecular units (icosahedra).<sup>132</sup>

The relative strength of the inter- and the intraicosahedral bonds has been related to the question of the compressibility of the icosahedral units with respect to the unit cell. High pressure neutron diffraction studies give direct evidence that the icosahedra are 23% more compressible than the intericosahedral space.<sup>120</sup> Compositional variation of longitudinal sound velocities<sup>75</sup> and pressure dependence of electrical resistivity<sup>97</sup> in boron carbide can also be interpreted in terms of soft icosahedra. Contradictory to these observations, theoretical simulations of the elastic properties of boron carbide at higher pressures predict lower compressibility of the icosahedra with respect to the unit cell.<sup>65,133</sup> Based on these results, Lazzari *et al.* argued that the intericosahedral bonds are *weaker* than the intraicosahedral ones, and challenged the notion of inverted molecular solid for boron carbide.<sup>65</sup> However, as noted by Shirai *et al.*,<sup>111</sup> these arguments did not take into consideration the fact that per each bond that connects an icosahedron to the surrounding lattice, there are ten bonds that connect atoms within the icosahedron. Because all available bonds contribute to the elastic deformation under hydrostatic compression, the 10-fold prevalence of the intraicosahedral bonds would result in lower compressibility of the icosahedron with respect to the lattice around it, even though individually intericosahedral bonds may be stronger.

The rigidity of the intrachain bond has also been debated, as evidence of significant displacements of the chain center atom in the direction perpendicular to the threefold axis, coming from X-ray and neutron diffraction measurements,<sup>71,34,78</sup> implied weak bonding between the chain center and the chain terminal atoms. Some researchers proposed that the weakness of this bond should arise from its presumably ionic character.<sup>134</sup> This apparent discrepancy with the conventional understanding and the results of theoretical modeling was addressed by Shirai,<sup>5</sup> who noted that the calculated restoring force against the displacement perpendicular to the bond axis would constitute only 10% of the bond stretching force, yielding a low energetic barrier for the chain center atom to move in the plane normal to the bond axis,

and at the same time preserving a strong force constant for atomic displacement in the axial direction. Additional evidence that supports the notion of intrachain bond softness comes from the spectral position of the bands at 480 and  $535\text{ cm}^{-1}$  observed in the Raman spectra of boron carbide, which are assigned to stretching vibrations in the CBC chains by researchers who endorse Emin's structural model.<sup>59</sup> The low frequency of these bands implies a weak force constant. However, assignment of these two bands to the CBC chain-stretching mode is questionable in view of a more recent theoretical analysis of the vibrational properties of boron carbide by Vast and co-workers,<sup>39,65</sup> who have demonstrated that between the two bands in question, only the  $480\text{ cm}^{-1}$  band was associated with the linear chain, and even this band had its origin in chain rotation and not in chain stretching, as discussed in Section III. As such, neither the Raman band at  $480\text{ cm}^{-1}$  nor the one at  $535\text{ cm}^{-1}$  would carry information on the axial rigidity of the intrachain bond.

Theoretical calculations find that the  $C_{11}$  elastic constant is higher than the  $C_{33}$  constant for both  $(\text{B}_{12})\text{CBC}$  (nominal  $\text{B}_{6.5}\text{C}$  stoichiometry) and  $(\text{B}_{11}\text{C})\text{CBC}$  (nominal  $\text{B}_4\text{C}$  stoichiometry) structural configurations.<sup>135</sup> This shows good agreement with a similar trend in the experimentally measured values of  $C_{11}$  and  $C_{33}$  obtained on a  $\text{B}_{5.6}\text{C}$  single crystal (Table III).<sup>136</sup> The commensurable magnitudes of  $C_{11}$  and  $C_{33}$  are at odds with the intuitive expectation that due to the alignment of the stronger intericosahedral bonds with the rhombohedral lattice vectors, the stiffness of the boron carbide crystal should be higher along the [001] direction rather than on the (001) plane, i.e.,  $C_{11}$  should be lower than  $C_{33}$ . Shirai *et al.*<sup>133</sup> explained this apparent contradiction in terms of internal relaxation of the boron carbide lattice under external stress. They noted that the distortion of the icosahedra due to their compressibility anisotropy should result in slight deviations of the intericosahedral bonds from the lattice vectors of the rhombohedral unit cell, as illustrated in Fig. 23. To accommodate deformation under compression along the [001] direction, the stiff intericosahedral bonds would choose to rotate instead of contracting, leading to relaxation of the entire crystal structure. The presence of a stiff intrachain bond will not prevent this relaxation because the chain itself is supported by bonds that lie near the (001) plane, and the stress is absorbed in this case by the chain-icosahedron bonds.

The anisotropy of boron carbide elastic properties was investigated on a  $\text{B}_{5.6}\text{C}$  single crystal using resonant ultrasound spectroscopy by McClellan *et al.*<sup>136</sup> Young's modulus  $E$  was found to be orientation independent when measured on the (111) plane (basal plane in hexagonal notation), but varied significantly when measured on prismatic (parallel to the [111] direction) and pyramidal planes (Fig. 24). The global maximum and minimum Young's moduli for the  $\text{B}_{5.6}\text{C}$  single crystal were found to be  $E_{\max} = 522\text{ GPa}$  and  $E_{\min} = 64\text{ GPa}$ , yielding an anisotropy ratio of  $E_{\max}/E_{\min} = 8.1$ . The global maximum Young's modulus was found to align with the [111] direction, implying higher stiffness of the crystal along the chain axis in response to tension or compression loading within the elastic regime. Shear modulus measured on the basal plane of the same crystal was found to be 165 GPa and

orientation independent; when measured on pyramidal and prismatic planes, shear modulus varied from the global minimum of  $G_{\min} = 165\text{ GPa}$  to the global maximum of  $G_{\max} = 233\text{ GPa}$  ( $G_{\max}$  along the [201] direction), yielding an anisotropy ratio of  $G_{\max}/G_{\min} = 1.4$  (Fig. 25).

Elastic properties of boron carbide have been shown to change with carbon content.<sup>3</sup> Table IV lists selected literature data for elastic moduli and Poisson's ratio of polycrystalline samples with different stoichiometries,<sup>75,117,120,136–138</sup> along with the theoretically calculated values of bulk modulus for the  $(\text{B}_{12})\text{CBC}$  and  $(\text{B}_{11}\text{C})\text{CBC}$  configurations.<sup>41,45,65,135</sup> Although caution should be exerted when comparing data for samples of different origin, the general trend is that the stiffness of boron carbide decreases at lower carbon concentrations. Compositional variations in Poisson's ratio do not follow this trend and span the range of 0.17 to 0.21, as reported by different groups.<sup>3,117,136</sup> Some of the earlier mechanical tests performed on hot-pressed boron carbide suggested that Young's modulus increased with decreasing carbon concentrations.<sup>23,139</sup> Gieske *et al.* used ultrasonic techniques to measure elastic properties of the samples with varying stoichiometries and observed a decrease in elastic moduli with the decrease in carbon concentration.<sup>75</sup> One

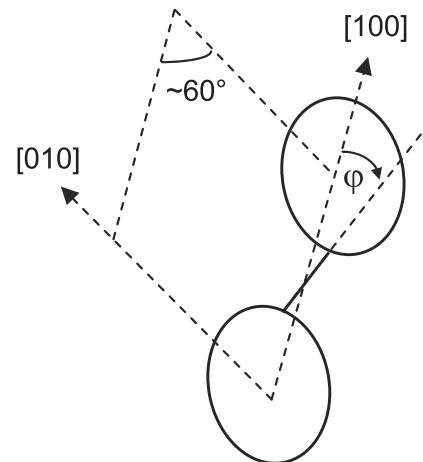


Fig. 23. Deformation of boron carbide icosahedra under stress after Shirai *et al.*<sup>133</sup> The intericosahedral bond (thick solid line) is deflected from the lattice direction [100] by an angle  $\varphi$ .

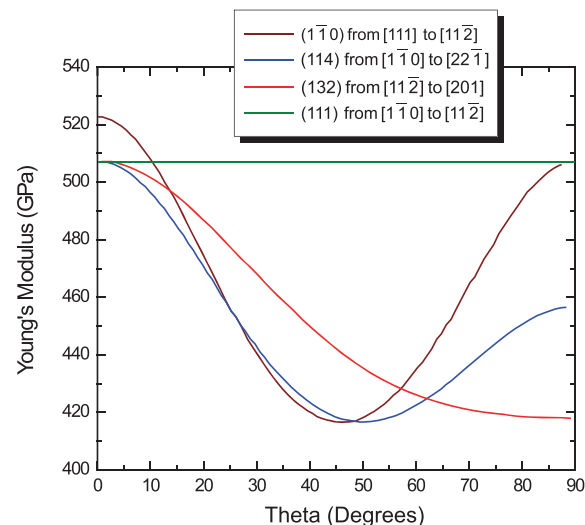
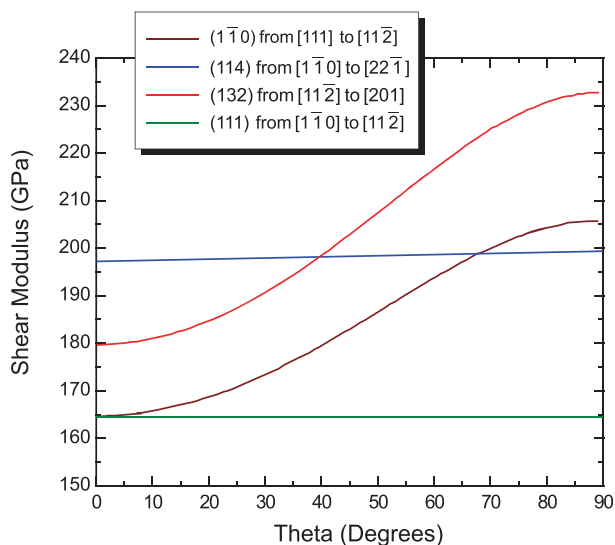


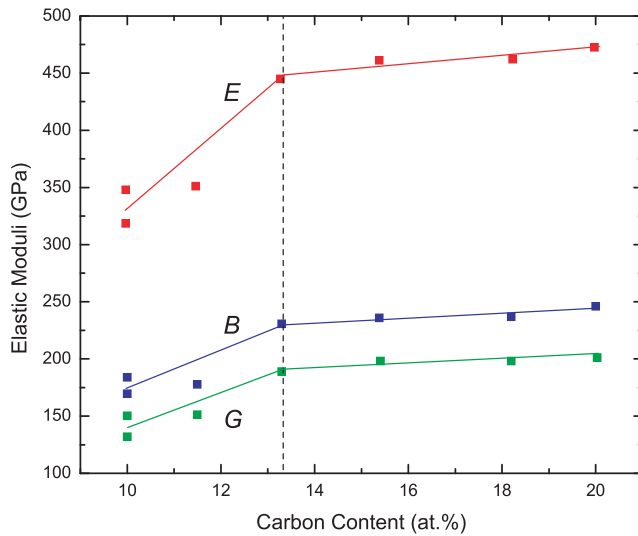
Fig. 24. The orientation dependence of the Young's modulus for  $\text{B}_{5.6}\text{C}$  single crystal. Reproduced from McClellan *et al.*,<sup>136</sup> with permission; ©2001 Springer.

Table III. Elastic Constants of Boron Carbide

Elastic constant $C_{ij}$ , GPa	McClellan <i>et al.</i> <sup>136</sup> (exp.)		Lee <i>et al.</i> <sup>135</sup> (calc.)	
	$\text{B}_{5.6}\text{C}$	$\text{B}_{6.5}\text{C}$	$\text{B}_4\text{C}$	
11	542.8	500.4	561.8	
33	534.5	430.2	517.7	
44	164.8			
12	130.6	125.3	123.6	
13	63.5	73.9	69.6	
14		7.7	17.8	



**Fig. 25.** The orientation dependence of the shear modulus for  $B_{5.6}C$  single crystal. Reproduced from McClellan *et al.*,<sup>136</sup> with permission; ©2001 Springer.



**Fig. 26.** The carbon content dependence of elastic moduli of hot-pressed boron carbide. Lines serve as guides to the eye. Data from Gieske *et al.*<sup>75</sup>

**Table IV. Compositional Dependence of Elastic Moduli and Poisson's Ratio in Boron Carbide**

Stoichiometry	at.% C	Bulk modulus [GPa]		Young's modulus exp.	Shear modulus exp.	Poisson's ratio exp.
		exp.	calc.			
$B_4C$	20.0	247 <sup>c</sup>	246 <sup>e</sup>	472 <sup>c</sup>	200 <sup>c</sup>	0.18 <sup>c</sup>
		235 <sup>e</sup>	234 <sup>g</sup>	462 <sup>e</sup>	197 <sup>e</sup>	0.17 <sup>e</sup>
		199 <sup>d</sup>	248 <sup>h</sup>	448 <sup>b</sup>	188 <sup>a</sup>	0.21 <sup>b</sup>
		239 <sup>j</sup>		441 <sup>a</sup>		
		220 <sup>d</sup>				
$B_{4.5}C$	18.2	237 <sup>c</sup>		463 <sup>c</sup>	197 <sup>c</sup>	0.17 <sup>c</sup>
$B_{5.6}C$	15.2	236 <sup>c</sup>		462 <sup>c</sup>	197 <sup>c</sup>	0.17 <sup>c</sup>
		237 <sup>f</sup>		460 <sup>f</sup>	195 <sup>f</sup>	0.18 <sup>f</sup>
$B_{6.5}C$	13.3	231 <sup>c</sup>	217 <sup>g</sup>	446 <sup>c</sup>	189 <sup>c</sup>	0.18 <sup>c</sup>
		227 <sup>i</sup>				
$B_{7.7}C$	11.5	178 <sup>c</sup>		352 <sup>c</sup>	150 <sup>c</sup>	0.17 <sup>c</sup>
$B_9C$	10.0	183 <sup>c</sup>		319 <sup>c</sup>	150 <sup>c</sup>	0.21 <sup>c</sup>
		130 <sup>c</sup>		348 <sup>c</sup>	132 <sup>c</sup>	0.16 <sup>c</sup>

(a)Schwetz and Grellner<sup>137</sup>

(b)Murthy<sup>138</sup>

(c)Gieske *et al.*<sup>75</sup>

(d)Nelmes *et al.*<sup>120</sup>

(e)Manghnani *et al.*<sup>117</sup>

(f)McClellan *et al.*<sup>136</sup>

(g)Lee *et al.*<sup>135</sup>

(h)Lazzari *et al.*<sup>65</sup>

(i)Guo *et al.*<sup>41</sup>

(j)Aydin and Simtek<sup>45</sup>

particularity of Gieske's data is the observed change in slope in the Young's modulus versus at. % C dependence at carbon concentrations of ~13 at. %, corresponding to the  $B_{6.5}C$  stoichiometry. Shear and bulk moduli exhibited a similar behavior, as shown in Fig. 26. A direct correlation can be drawn between these observations and a kink in the carbon dependence of the  $c$  lattice parameter (Fig. 3), which is believed to be indicative of the distinct mechanisms for substitution of boron atoms into the icosahedral and the chain units that take place at the boron- and the carbon-rich sides of the  $B_{6.5}C$  composition.

Manghnani *et al.* investigated the pressure dependence of the elastic moduli of polycrystalline boron carbide up to 2.1 GPa, finding a nearly linear relationship as shown in Fig. 27.<sup>117</sup> The measured bulk moduli were consistent with

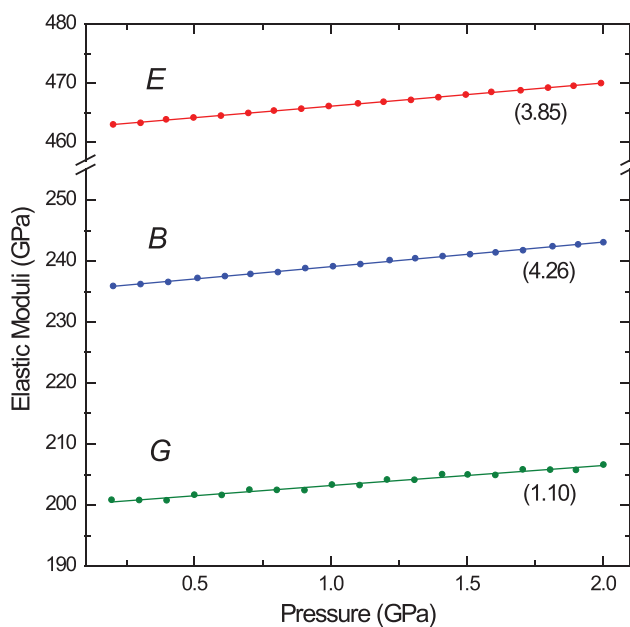


**Fig. 27.** Pressure dependence of bulk modulus  $B$ , Young's modulus  $E$ , and shear modulus  $G$  in hot pressed boron carbide. Lines are linear fits to the data. Respective pressure coefficients are shown in parentheses. Reproduced from Manghnani *et al.*,<sup>117</sup> with permission; ©2000 Universities Press (India) Limited.

the values obtained by Nelmes *et al.* in high pressure neutron diffraction studies on boron carbide.<sup>120</sup> The pressure dependence of boron carbide bulk properties can be understood from the inverted molecular solid concept described above.

In contrast to the elastic moduli that are intrinsic properties of the material and derive from atomic bonding, mechanical properties (hardness, strength, fracture toughness, etc.) strongly depend on such external factors as quality and size of the sample, size of the grains, porosity, presence of defects and flaws, conditions of loading, etc. This is one of the reasons for significant variations in the reported hardness values for boron carbide. Generally, Knoop hardness is used as a reference, with tests under a 200 g loading resulting in a value of HK<sub>200</sub> between 29 and 31 GPa.<sup>1,3,24</sup> Vickers hardness of boron carbide is generally ~30% higher, although the

values of  $VH_{100}$  as high as 47 GPa have been reported in the samples prepared by chemical vapor deposition (CVD) technique.<sup>140</sup> In nanoindentation measurements on  $B_{4.3}C$  single crystals, Berkovich hardness values of 41–42 GPa have been measured by different groups.<sup>114,141</sup> This impressive hardness ranks boron carbide as third overall hardest material known, behind diamond and cubic boron nitride. Several works report that boron carbide hardness increases with the carbon content until the edge of the homogeneity range is reached,<sup>26,140,142,143</sup> at carbon concentrations in excess of 20%, hardness rapidly falls off due to precipitation of the carbon phase from the  $B_4C$  solid solution.<sup>140</sup>

Boron carbide is characterized by flexure strength values on the order of 350 MPa.<sup>1,3,24</sup> Density of boron carbide varies with carbon concentration as  $\rho = 2.422 \text{ g/cm}^3 + 0.0048 \cdot [\text{at.\% C}]$ , with a commonly reported value of 2.52 g/ $\text{cm}^3$  corresponding to the  $B_4C$  stoichiometry.<sup>1</sup> This combination of high strength and low density makes boron carbide one of the most attractive structural materials known. As expected of both a ceramic and a strong material, boron carbide has relatively low fracture toughness. Values of  $K_{IC}$  for boron carbide are given at  $\sim 1.3 \text{ MPa}\cdot\text{m}^{1/2}$ .<sup>1,3,144</sup>

There is considerable interest in the application of boron carbide as lightweight armor material due to its exceptional hardness, outstanding elastic properties and low theoretical density. From the ballistic viewpoint, of particular interest is the response of boron carbide to shock loading. However, available shock loading data show that the performance of boron carbide at high velocity, high pressure impact is much lower than that expected from its superior static mechanical properties. The shear strength of boron carbide in the shocked state (Fig. 28) falls off rapidly above the HEL,<sup>145,146</sup> indicating premature failure of the material as the shock stress reaches a threshold value of  $\sim 20$  GPa. This behavior is similar to the shock response of single crystal  $Al_2O_3$ ,<sup>147,148</sup> where the drop in the shear strength has been linked to a stress-induced phase transformation, and is markedly different from the shock response of other armor ceramic materials, such as  $SiC$ <sup>149–151</sup> and polycrystalline  $Al_2O_3$ ,<sup>147,149,152</sup> which are characterized by the deformation hardening that commences immediately above the HEL. Apart from a possible phase transformation, the anomalous decrease in shear strength of boron carbide beyond the HEL may be related to a catastrophic propagation of microcracks and other micro-

structural defects, leading to material's collapse behind the elastic precursor wave.

## V. Stress-Induced Structural Instability

The possibility of a phase transformation in boron carbide under shock loading has been discussed in the literature to a considerable extent. Figure 29 shows the available experimental shock compression data for boron carbide of varying starting density as reported by different authors.<sup>146,153–158</sup> Grady<sup>159,160</sup> identifies three distinct regions in the hydrodynamic equation of state of boron carbide, each corresponding to the hydrodynamic compression of a particular phase: an ambient phase, a second phase that exists in the pressure range of 25–35 to 45–55 GPa, and a third phase beyond 45–55 GPa [Fig. 29(a)]. Vogler *et al.*<sup>146</sup> note that a possible phase transition may correspond to the intercept point between the hydrostatic and the hydrodynamic compression curves which occurs at  $\sim 40$  GPa in boron carbide [Fig. 29(b)]. Mashimo and co-workers discuss three regions in the Hugoniot compression data: a region of predominantly elastic deformation below the HEL ( $\sim 20$  GPa), a region of mostly isotropic compression from  $\sim 20$  to 38 GPa, and a region of isothermal compression that extends beyond 38 GPa.<sup>158</sup> An onset of a phase transformation in boron carbide, according to this group, corresponds to a kink in the Hugoniot compression curve between the isotropic and the isothermal compression regimes [Fig. 29(c)]. Both Vogler *et al.*<sup>146</sup> and Zhang *et al.*<sup>158</sup> also report that the ambient bulk sound velocity in boron carbide is significantly higher than the shock velocity at the intercept pressure, which is consistent with the concept of a phase transformation. Another possible piece of evidence for a shock-induced phase change in boron carbide, according to Vogler *et al.*, is a very steep drop in particle velocity observed during initial unloading in release experiments, which could be associated with a reverse transformation that occurs immediately upon unloading.<sup>146</sup> All the results discussed above are highly suggestive of a phase transformation in boron carbide under shock loading, albeit not entirely conclusive.

The damage mechanism responsible for the failure of boron carbide under shock loading has been directly assessed by Chen *et al.*<sup>161</sup> High resolution transmission electron microscopy (HR TEM) analysis of boron carbide ballistic targets subjected to supercritical impact velocities and pressures in excess of 20–23 GPa revealed the formation of 2–3 nm wide intragranular amorphous bands that occurred parallel to specific crystallographic planes and contiguous with the apparent cleaved fracture surfaces (Fig. 30). At subcritical impacts, the amorphous bands were never observed; instead, a relatively high density of stacking faults and microtwins suggested plastic deformation of the material under shock loading.<sup>161</sup>

Stress-induced structural transformation of boron carbide has been reported in static indentation,<sup>114,141,162</sup> dynamic indentation,<sup>163,164</sup> and scratching experiments.<sup>162,165</sup> Fig. 31 shows an example of HR TEM observations of large amorphized zones formed within the indentation contact area and in the scratch debris in  $B_{4.3}C$  single crystal.<sup>162</sup> Within the amorphous zone, nanosized grains of crystalline material with retained orientation are present, which could indicate highly anisotropic deformation of boron carbide under stress. Formation of nanosized oriented amorphous bands similar to the bands observed in ballistically impacted material (Fig. 30) has also been reported for indented boron carbide.<sup>162</sup> Electron energy loss spectroscopy (EELS) observations indicate that the amorphous structure such as the boxed area 2 in Fig. 31(b) shows a different carbon  $K$  edge compared to the crystalline lattice. The appearance of an enhanced  $\pi^*$  peak in the carbon  $K$  edge implies  $sp^2$  bonding, i.e., carbon double bonding in the material. Unlike the carbon edge, the core-loss edge of boron shows little fundamen-

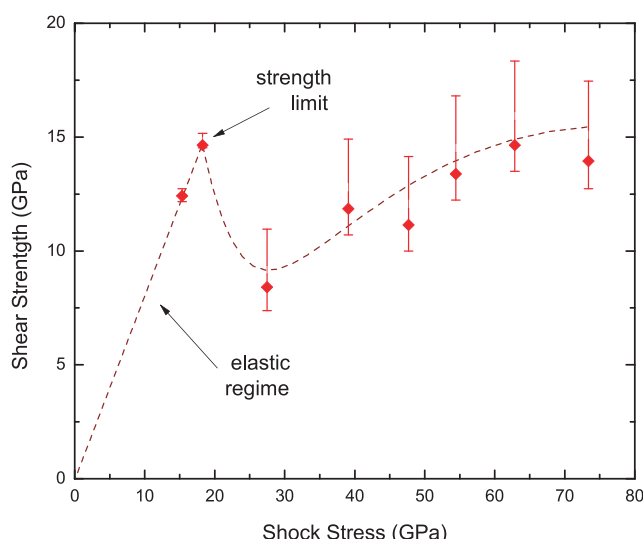


**Fig. 28.** Shear strength of boron carbide in the shocked state, estimated from reshock and release experiments. Line serves as a guide to the eye. Reproduced from Vogler *et al.*,<sup>146</sup> with permission; ©2004 American Institute of Physics.

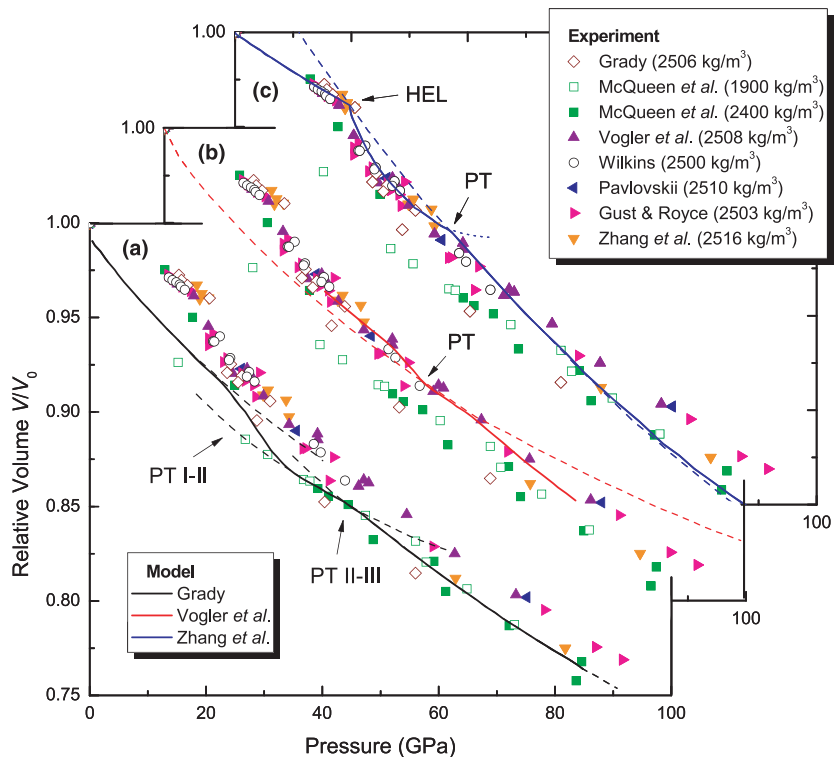


**Fig. 29.** Shock compression data on boron carbide as reported by Wilkins,<sup>153</sup> McQueen *et al.*,<sup>154</sup> Pavlovskii,<sup>155</sup> Gust and Royce,<sup>156</sup> Grady,<sup>157</sup> Vogler *et al.*,<sup>146</sup> and Zhang *et al.*<sup>158</sup> (symbols) and selected model representations accounting for phase transformations (lines). (a) Grady's model,<sup>160</sup> dash lines, hydrodynamic compression curves for phase I (below 25–35 GPa), phase II (25–35 GPa to 45–55 GPa), and phase III (beyond 45–55 GPa); solid line, a composite hydrodynamic compression curve. (b) Model of Vogler *et al.*<sup>146</sup>; dash line, extrapolation of hydrostatic compression data of Manghnani *et al.*<sup>117</sup>; solid line, mean pressure from reshock and release experiments.<sup>146</sup> (c) Model of Zhang *et al.*<sup>158</sup>; dash line, isothermal compression curve; dot line, isotropic compression curve; solid line, Hugoniot compression curve. Suggested phase transition (PT) points and the Hugoniot elastic limit (HEL) for boron carbide are indicated by arrows.

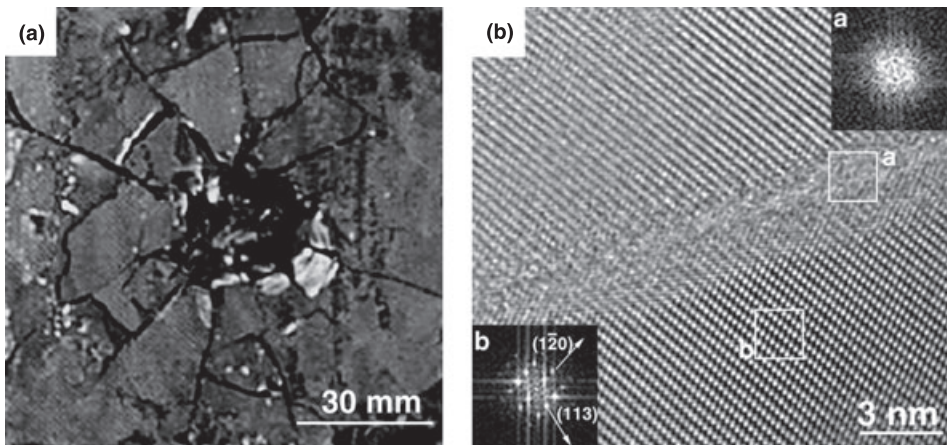


**Fig. 30.** (a) Boron carbide ballistic target that comminuted during impact and (b) an HR TEM image of a fragment produced by a ballistic test at impact pressure of 23.3 GPa. The lattice images on either side of the band in (b) correspond to the [101] direction of crystalline boron carbide, and the loss of lattice fringes in the band indicates localized amorphization. Reproduced from Chen *et al.*,<sup>161</sup> with permission; ©2003 The American Association for the Advancement of Science.

tal changes.<sup>162</sup> Therefore, it is inferred that the boron atoms retain their chemical state, while the chemical state of carbon is partially modified during indentation.

These observations are corroborated by extensive Raman spectroscopy data collected on boron carbide samples subjected to high stresses associated with various types of contact-loading situations.<sup>114,141,162,163,165</sup> Indication of the structural changes is evidenced by the appearance of high-frequency bands at 1330, 1520, and 1810 cm<sup>-1</sup> in the Raman spectra of indented boron carbide (Fig. 32). The alterations of the Raman spectra are independent on the quality of the starting material: identical bands are observed in the single

crystals and in the polycrystalline samples after indentation at comparable loads [Figs. 32(b) and (e)]. Also shown in Fig. 32(d) is the Raman spectrum of a carbonaceous inclusion in polycrystalline boron carbide; such inclusions are common in hot-pressed samples and are not to be confused with the Raman features of the transformed amorphous boron carbide.

Spectral position of the 1330 and 1520 cm<sup>-1</sup> bands, as well as the dispersive character of the 1330 cm<sup>-1</sup> band (Fig. 33), imply the correlation of these bands with, respectively, the *D* and the *G* bands of amorphous/graphitic carbon. However, this explanation may be in conflict with the

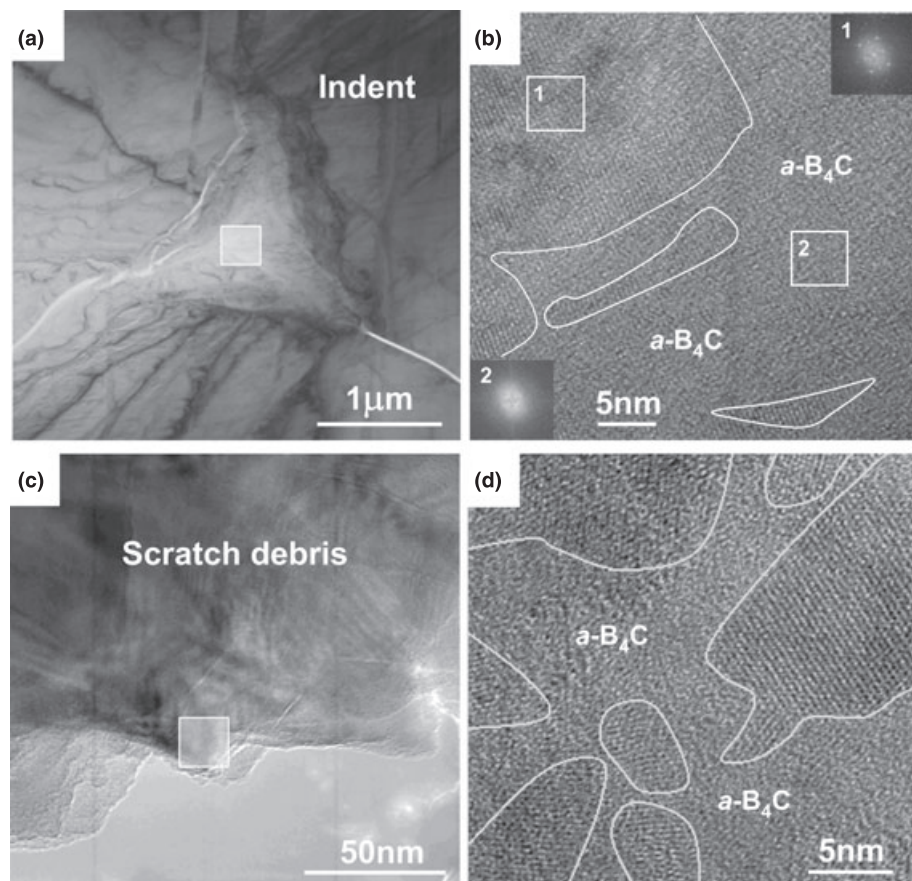


**Fig. 31.** Plain view TEM micrographs of (a) a 100 mN Berkovich indent and (b) scratch debris in single crystal  $B_{4.3}C$ . (c,d) Magnified high resolution lattice images of the boxed areas in (a,b) showing the presence of amorphous material. Reproduced from Ge *et al.*,<sup>162</sup> with permission; ©2004 Elsevier.

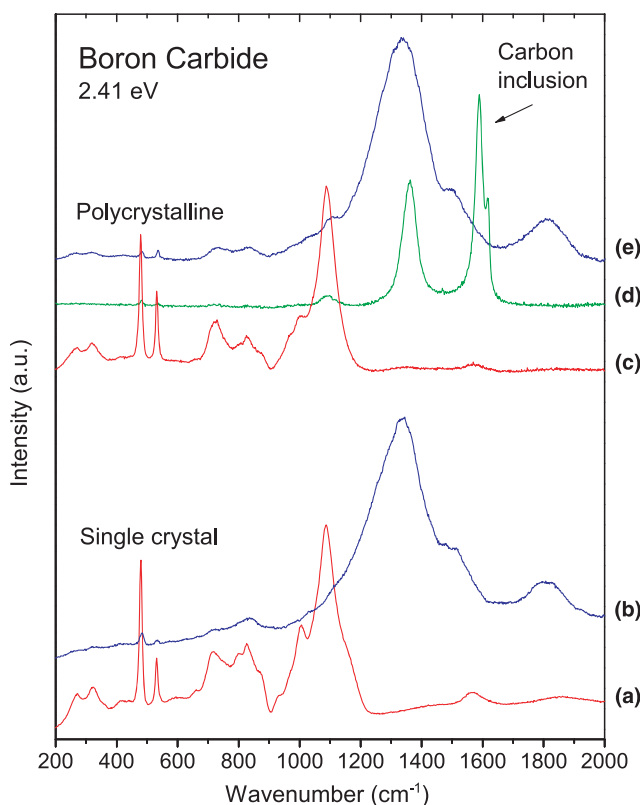


**Fig. 32.** Raman spectra of (a) pristine and (b) indented single crystal  $B_{4.3}C$ , and (c) pristine and (e) indented polycrystalline hot-pressed boron carbide. Raman spectrum of a graphitic inclusion in polycrystalline boron carbide is shown in (d).

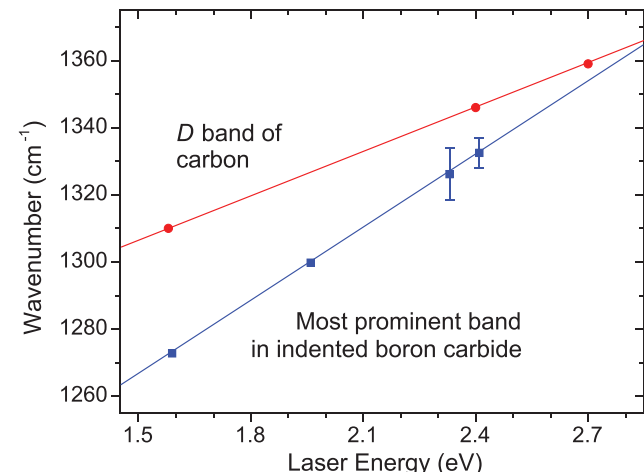


**Fig. 33.** Dependence of the most prominent band in the Raman spectra of indented single crystal  $B_{4.3}C$  (squares) on laser excitation energy in comparison with a similar dependence of the *D* band of disordered carbon (circles, data from Pócsik *et al.*).<sup>166</sup> Lines are linear fits to the data. Reproduced from Domnich *et al.*,<sup>114</sup> with permission; ©2002 American Institute of Physics.

following observations: (i) the intensity of the *D* band of disordered carbon increases with the increasing excitation wavelength,<sup>166</sup> while the band at  $\sim 1330 \text{ cm}^{-1}$  does not show such dependence;<sup>114</sup> (ii); the *G* band is a prominent band in all carbon structures involving  $sp^2$  bonding<sup>167</sup> and the *D/G* intensity ratio in disordered/amorphous carbon never exceeds 2.5,<sup>128</sup> whereas the intensities ratio for the bands at  $\sim 1330$  and  $\sim 1520 \text{ cm}^{-1}$  varies in the range of 4–5 at room tempera-

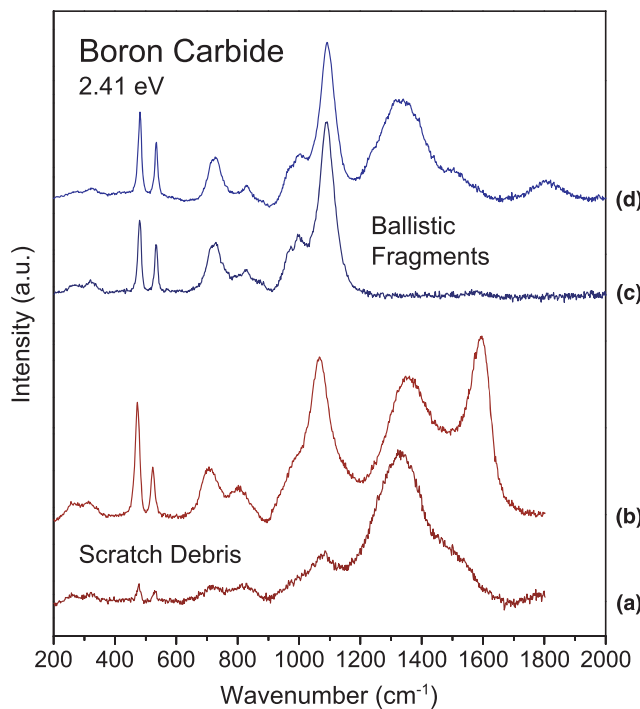


**Fig. 34.** Raman spectra of hot-pressed boron carbide subjected to (a,b) scratching<sup>162</sup> and (c,d) ballistic impact. Scratch debris consistently shows evidence of amorphous material (a), and is found to graphitize upon annealing (b). Most analyzed locations on the ballistic fragment surfaces yield spectra similar to (c); however, formation of amorphous material can also be observed, as evidenced by the Raman spectrum in (d).

ture,<sup>114,141</sup> and (iii) the position of the band at  $\sim 1520 \text{ cm}^{-1}$  (Fig. 32) is strongly downshifted compared to the G band of graphite.<sup>167</sup> It is also important to note that the Raman band at  $\sim 1520 \text{ cm}^{-1}$  that appears in the deformed material is not necessarily related to the  $1570 \text{ cm}^{-1}$  band in the Raman spectra of pristine boron carbide [Fig. 32(a)], which has been attributed in the literature to the presence of carbonaceous inclusions in boron carbide samples, or, alternatively, to the vibrations of the CBB chains.<sup>60,116</sup>

Changes in the Raman spectra indicative of formation of the amorphous material are also observed for the samples subjected to dynamic loading, ranging from scratching [Fig. 34(a)] to ballistic impact [Figs. 34(c) and (d)]. Ge *et al.* noted that annealing of the scratch debris with the laser beam leads to appearance of the G band in the Raman spectrum of amorphous boron carbide [Fig. 34(b)], implying graphitization of the transformed material.<sup>162</sup> Effect of temperature on the Raman features of amorphous boron carbide was systematically studied by Yan *et al.*<sup>141</sup> While cryogenic temperatures were found to have no effect on the Raman spectra, the main features of the amorphous boron carbide (bands at 1330, 1520, and  $1810 \text{ cm}^{-1}$ ) were gradually decreasing under heating until their final disappearance at  $400^\circ\text{C}$ – $500^\circ\text{C}$ , as shown in Fig. 35. This was accompanied by a gradual increase in the intensity of the G band at  $1586 \text{ cm}^{-1}$ . Yan *et al.* argued that the stress-induced amorphization of boron carbide could be mainly accomplished through the structural change of the CBC chains, with the small amount of boron in the chains residing in the aromatic rings by substituting carbon, and the ( $\text{B}_{11}\text{C}$ ) icosahedra preserving their structure. Further, this group associated the qualitative changes that occurred in the Raman spectra around  $\sim 500^\circ\text{C}$  with the rapid coagulation of the small  $sp^2$  bonded carbon clusters that had presumably formed during room-temperature indentation, and formation of larger-size carbon domains.<sup>141</sup>

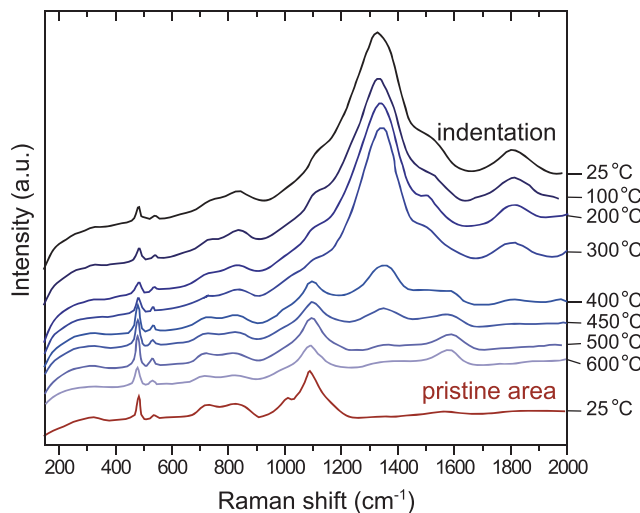


**Fig. 35.** Effect of annealing on the evolution of the Raman spectra of a hardness indent in single crystal  $\text{B}_{4.3}\text{C}$ . The spectra were acquired at temperatures ranging from 25°C (ambient) to 600°C. An ambient-temperature spectrum of a pristine  $\text{B}_{4.3}\text{C}$  surface is shown for reference. Reproduced from Yan *et al.*,<sup>141</sup> with permission; ©2006 American Institute of Physics.

However, this structural model for amorphous boron carbide resides on an assumption that the 1330 and 1520  $\text{cm}^{-1}$  bands are identical to the D and the G bands of carbon; this is not necessarily true for the reasons discussed above. As an additional argument against this assumption, deconvolution of the high frequency bands in the Raman spectra in Fig. 35 shows that the intensity of the 1520  $\text{cm}^{-1}$  feature in the spectrum of amorphous boron carbide decreases independently of the graphitic G band that appears at 1586  $\text{cm}^{-1}$  at elevated temperatures; in the temperature range of 300°C–450°C, both these bands are present in the spectra, indicating their different origins. Generally, the Raman spectra of amorphous boron carbide and amorphous/graphitic carbon are qualitatively different in terms of band frequencies, band widths, and relative band intensities, as evidenced from a direct comparison of the Raman spectra in Figs. 32(d) and (e). A mere appearance of graphitic D and/or G bands in stressed boron carbide should not be necessarily interpreted as a sign of amorphization; rather, the presence of a smaller band at 1810  $\text{cm}^{-1}$  must be used as a reliable indication of a completed structural transformation.

Interestingly, the Raman spectra of amorphous boron carbide films prepared by magnetron sputtering<sup>168,169</sup> exhibit distinctly different features and resemble a broadened spectrum of crystalline boron carbide with the major band centered around 1100  $\text{cm}^{-1}$  (Fig. 36). In addition, the bands at  $\sim 1330 \text{ cm}^{-1}$  and  $\sim 1520 \text{ cm}^{-1}$  are never observed in amorphous boron carbide films.<sup>169</sup> This suggests the possibility for an existence of two distinct forms of amorphous boron carbide consisting of a distorted icosahedral network and different arrangements of carbon and boron atoms that link the icosahedra together.

This problem was addressed in a theoretical study of amorphous boron carbide by Ivashchenko *et al.*<sup>44</sup> In this work, two forms of amorphous B–C networks, one based on a 120-atom rhombohedral  $\text{B}_4\text{C}$  cell (*a*-120), and the other one based on a 135-atom hypothetical cubic  $\text{B}_4\text{C}$  cell (*a*-135), were simulated by means of molecular dynamic (MD) methods. The *a*-120 configuration was found to consist of disordered icosahedra composed mainly of boron atoms connected by topologically disordered B–C and C–C networks. The structure of the *a*-135 configuration was found to be similar to the one of *a*-120, but it was lacking the eight-fold coordinated atoms, implying a less random amorphous

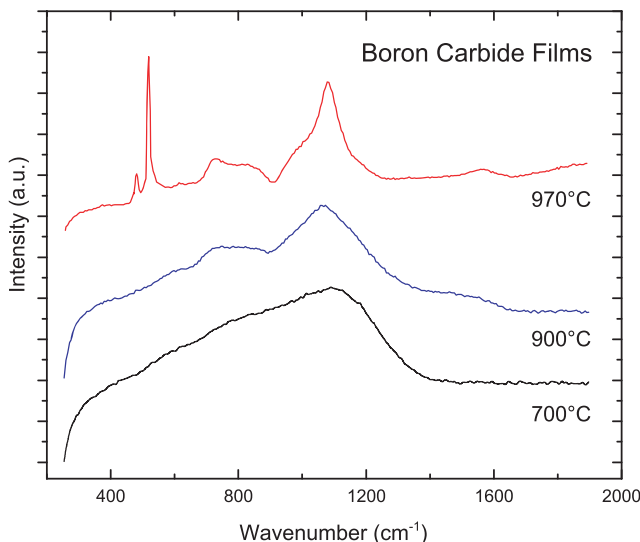


**Fig. 36.** Raman spectra of boron carbide films deposited by magnetron sputtering at temperatures of 700°C, 900°C, and 970°C.<sup>168</sup> Crystallization of the films occurs at temperatures above 900°C.

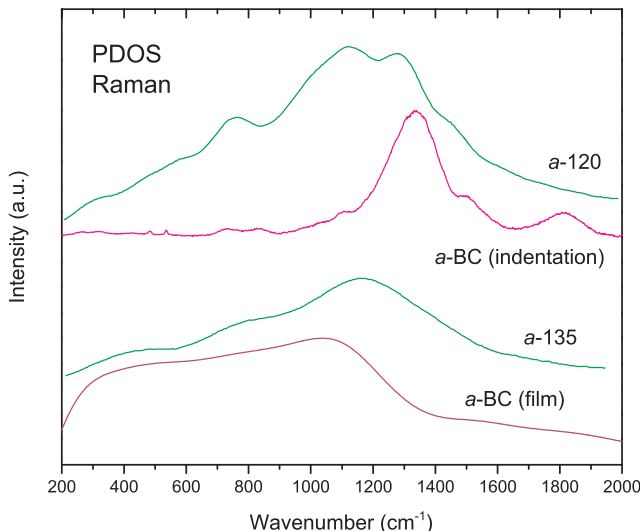


**Fig. 37.** Comparison of the calculated PDOS of the amorphous *a*-120 and *a*-135 structures<sup>44</sup> with the experimental Raman spectra of the indented boron carbide (this work) and an amorphous boron carbide film prepared by magnetron sputtering.<sup>169</sup>

network. The simulated phonon densities of states for the two amorphous networks are compared with the experimental Raman spectra obtained on indented boron carbide crystals and those measured on amorphous boron carbide films in Fig. 37. In the calculated PDOS, the band at 1800 cm<sup>-1</sup> is missing in both the *a*-120 and the *a*-135 configurations. For the *a*-120 network, the two PDOS bands at 1290 and 1450 cm<sup>-1</sup> resemble the two prominent features in the Raman spectra of indented boron carbide [Fig. 37(a)], and the band at 750 cm<sup>-1</sup> correlates with the increased density of the icosahedral modes in the PDOS calculated for the crystalline (B<sub>12</sub>)CBC form, as shown in Fig. 16(b). In contrast, the PDOS of the *a*-135 network shows a general correlation with the broad features in the Raman spectra of amorphous boron carbide films [Fig. 37(a)]. These results provide basis for a thesis that the stress-induced transformation of boron carbide proceeds via destruction of the linear chains, formation of topologically disordered B-C and C-C networks from the chain C and B atoms, distortion of the icosahedral (B<sub>12</sub>) and (B<sub>11</sub>C) units, and rearrangement of these structural elements into a randomly interconnected amorphous network.

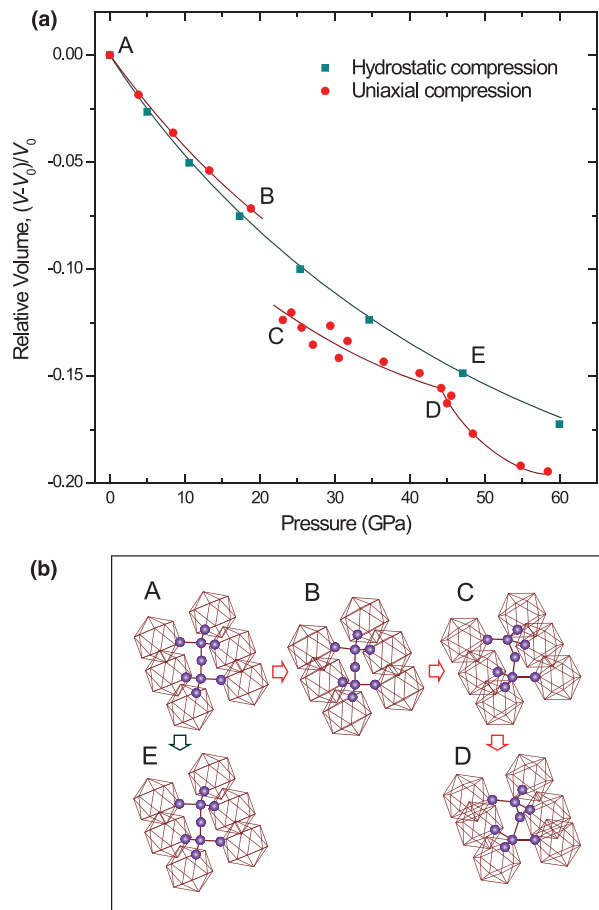


**Fig. 38.** *Ab initio* simulation of the stabilization of B<sub>11</sub>C(CBC) under hydrostatic and uniaxial compression. (a) Compressed volume versus pressure. The square data represent the volume change with hydrostatic pressure, and the circle data correspond to the volume change with uniaxial stress along the CBC atomic chain. (b) Atomic configurations of the B<sub>4</sub>C unit cell at various pressures corresponding to data points in (a). Reproduced from Yan *et al.*,<sup>118</sup> with permission; ©2009 American Physical Society.

The driving force for such structural collapse is still to be established. Yan *et al.* addressed this issue from the experimental position.<sup>118</sup> A complete set of experiments using quasi-hydrostatic and quasi-uniaxial compression up to 50 GPa, followed by depressurization to ambient pressure, was conducted on a boron carbide single crystal, and *in situ* Raman spectroscopy was engaged to detect possible high pressure phase transformations. It was observed that under hydrostatic compression, the material remained a perfect single crystal without visible surface relief and cracking; no evidence of amorphization was detected in the samples loaded hydrostatically after pressure release. The results were significantly different when the single crystal boron carbide was subjected to uniaxial loading and unloading. In this case, the depressurized samples were found to be broken into a number of smaller fragments; evident cracks, surface relief, and shear bands could be observed optically; and the formation of amorphous material was evidenced by *in situ* Raman spectroscopy at 13–16 GPa during unloading of the samples that had been previously loaded to pressures in excess of 25 GPa. Further, Raman spectroscopy analysis of the fully depressurized samples revealed spectral features typical for stress amorphized material as observed in indentation and scratching experiments, i.e., the bands at ~1330, ~1520, and ~1820 cm<sup>-1</sup>. These results emphasized the importance of nonhydrostatic stresses for the stability of boron carbide at high pressure.

Theoretical simulations by the same group indicated a drastic volume change of the hypothetical (B<sub>11</sub>C)CBC unit

cell at the destabilization pressure of 19 GPa (consistent with the HEL of 15–20 GPa) due to the bending of the CBC chain (Fig. 38).<sup>118</sup> At higher pressures, the chain deformation was found to continue until the  $(B_{11}C)$ CBC lattice was irreversibly distorted. It was suggested that the central boron atom of the chain could bond with the neighboring atoms in the icosahedra forming a higher energy structure. The release of this energy during depressurization was proposed to be responsible for the collapse of the boron carbide structure and the formation of localized amorphized bands.<sup>118</sup>

Theoretical investigation of phase stability in boron carbide polytypes at elevated pressures was conducted by Fanchini *et al.*<sup>40</sup> The free energies for several boron carbide configurations were calculated under increasing hydrostatic pressure at room temperature. The results indicated that the energetic barrier for pressure-induced amorphization of boron carbide was by far the lowest for the hypothetical  $(B_{12})$ CCC polytype, which was found to be unstable at

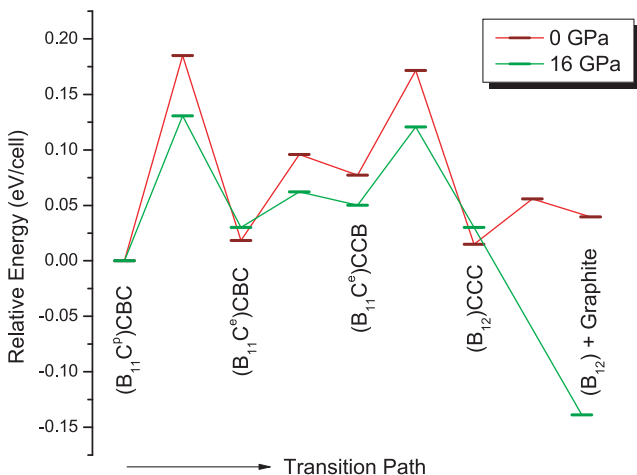


**Fig. 39.** A schematic route proposed by Fanchini *et al.*<sup>40</sup> to transform  $(B_{11}C^p)$ CBC into  $(B_{12})$  and graphite at ambient pressure and at 16 GPa. The transformation steps involve migration of the carbon atom in the icosahedron from a polar to an equatorial site,  $(B_{11}C^p)$ CBC  $\rightarrow$   $(B_{11}C^e)$ CBC; migration of the boron atom in the chain from the central to a boundary site,  $(B_{11}C^e)$ CBC  $\rightarrow$   $(B_{11}C^e)$ CCB; swapping of the equatorial icosahedral carbon atom with the boundary boron atom in the chain,  $(B_{11}C^e)$ CBC  $\rightarrow$   $(B_{12})$ CCC; and coalescence of the obtained CCC chains along the (113) planes, through rotation of their axis around the [001] direction.

6–7 GPa during hydrostatic loading. The collapse of the  $(B_{12})$ CCC structure was predicted to result in a segregation of the  $(B_{12})$  icosahedra and amorphous carbon in the form of 2–3 nm wide bands along the (113) lattice direction, in agreement with the TEM observations on ballistically loaded samples shown in Fig. 30. An example of the most energetically favored transformation path of the  $(B_{11}C^p)$ CBC polytype into the  $(B_{12})$  icosahedra and graphitic carbon, as proposed by Fanchini *et al.*,<sup>40</sup> is schematically shown in Fig. 39 for two different values of hydrostatic pressure.

Both models discussed above are open to criticism. The results of Fanchini *et al.*<sup>40</sup> predict collapse of the  $(B_{12})$ CCC polytype under compression at hydrostatic pressures of only 6–7 GPa, but experimentally the ambient phase of boron carbide has been reported stable under hydrostatic compression of up to 100 GPa.<sup>118–120,122</sup> In line with the available experimental work, *ab initio* modeling by another group estimated the amorphization pressure for the  $(B_{12})$ CCC polytype to be at 300 GPa,<sup>44</sup> by far exceeding the predictions of Fanchini *et al.*<sup>40</sup> Moreover, there is compelling evidence that the  $(B_{12})$ CCC configuration does not exist in nature (e.g., Dekura *et al.*,<sup>86</sup> see also relevant discussion in Sections I and II). Fanchini *et al.* also predict the decomposition of the  $(B_{11}C^p)$ CBC polytype into the  $(B_{12})$  icosahedra and amorphous carbon at  $\sim$ 40 GPa,<sup>40</sup> which is more in line with the available shock compression and nanoindentation data on boron carbide, but once again finds no confirmation in the hydrostatic compression experiments. On the other hand, the model of chain bending under uniaxial compression proposed by Yan *et al.*,<sup>118</sup> albeit taking into account the importance of nonhydrostatic loading for the collapse of boron carbide, is lacking an empirical validation. This model assumes a transformation into a new structure in the loading stage, and the *in situ* Raman data obtained by the same group do not show any sign of such transformation. Nanoindentation data could provide information on volumetric changes associated with a transformation of this kind, particularly in view of consistent observation of the transformed material in the hardness imprints.<sup>170</sup> However, a discontinuity or a change in the slope of the loading curve that could be associated with a stress-induced transformation has never been recorded in boron carbide under depth-sensing indentation.<sup>114,171</sup> In addition, the signs of a reverse transformation, evidenced in the Yan's high pressure experiments,<sup>118</sup> could not be discerned in the nanoindentation unloading curves (Fig. 40). This may be related to very small volumetric changes associated with the presumed transformation, which is not surprising noting the small size of the transformed amorphized zones observed under the TEM (Figs. 30 and 31). Additional experimental and theoretical work will be required to fully

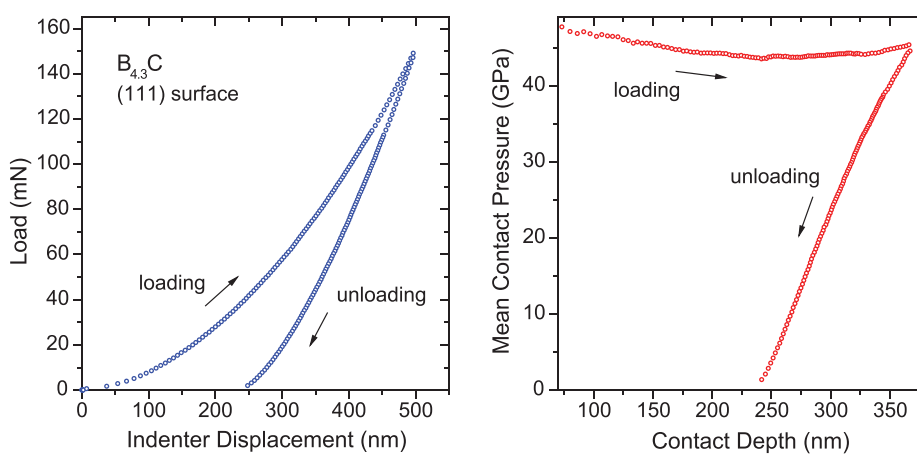


**Fig. 40.** Nanoindentation load versus displacement and mean contact pressure versus contact depth curves for the (111) surface of  $B_{4.3}C$ . The pressure is highest at the point of initial contact and decreases to 44 GPa at the end of the loading stage. The smooth line profile on both loading and unloading indicates the absence of sudden volumetric changes that could be associated with a phase transformation.

understand the stability of boron carbide under external loading, and the role of structural and compositional variations in defining the limits for boron carbide performance.

### Acknowledgments

The authors are thankful to Yury Gogotsi, Daibin Ge, and Thomas Juliano of Drexel University, Giovanni Fanchini, Varun Gupta, and Daniel Maiorano of Rutgers University, James McCauley and Jerry LaSalvia of the U.S. Army Research Laboratory for providing valuable insights and collaboration on this work. The authors also would like to express their gratitude to the anonymous reviewers for their constructive comments and illuminating ideas, particularly so in regard of the notion of boron carbide as a frustrated system.

### References

- 1A. Lipp, "Boron Carbide: Production, Properties, Application," *Tech. Rundsch.*, **58** [7] 1–47 (1966).
- 2J. L. Hoard and R. E. Hughes, "Elemental Boron and Compounds of High Boron Content: Structure, Properties, and Polymorphism"; pp. 26–153 in *The Chemistry of Boron and Its Compounds*, Edited by E. L. Muetterties. Wiley, New York, 1967.
- 3F. Thevenot, "Boron Carbide – A Comprehensive Review," *J. Eur. Ceram. Soc.*, **6**, 205–25 (1990).
- 4N. Vast, J. Sjakste, and E. Betranhandy, "Boron Carbides from First Principles," *J. Phys. Conf. Ser.*, **176**, 012002 (2009).
- 5K. Shirai, "Electronic Structures and Mechanical Properties of Boron and Boron-Bich Crystals (Part I)," *J. Superhard Mater.*, **32** [3] 205–25 (2010).
- 6K. Shirai, "Electronic Structures and Mechanical Properties of Boron and Boron-Bich Crystals (Part II)," *J. Superhard Mater.*, **32** [5] 336–45 (2010).
- 7A. K. Suri, C. Subramanian, J. K. Sonber, and T. Murthy, "Synthesis and Consolidation of Boron Carbide: A Review," *Int. Mater. Rev.*, **55** [1] 4–40 (2010).
- 8H. Werheit, V. Filipov, U. Kuhlmann, U. Schwarz, M. Armbruster, A. Leithe-Jasper, T. Tanaka, I. Higashi, T. Lundstrom, V. N. Gurin, and M. M. Korsukova, "Raman Effect in Icosahedral Boron-Rich Solids," *Sci. Technol. Adv. Mat.*, **11** [2] 023001 (2010).
- 9N. S. Hosmane, J. A. Maguire, and Z. Yinghuai, "Polyhedral Boron Cage Compounds: An Account," *Main Group Chem.*, **5** [4] 251–65 (2006).
- 10E. D. Jemmis and M. M. Balakrishnarajan, "The Ubiquitous Icosahedral B<sub>12</sub> in Boron Chemistry," *B. Mater. Sci.*, **22** [5] 863–7 (1999).
- 11B. Morosin, G. H. Kwei, A. C. Lawson, T. L. Aselage, and D. Emin, "Neutron Powder Diffraction Refinement of Boron Carbides. Nature of Intericosahedral Chains," *J. Alloy. Compd.*, **226** [1–2] 121–5 (1995).
- 12J. Jiménez, D. G. J. Sutherland, T. van Buuren, J. A. Carlisle, L. J. Terminiello, and F. J. Himpel, "Photoemission and X-Ray-Absorption Study of Boron Carbide and Its Surface Thermal Stability," *Phys. Rev. B*, **57** [20] 13167–74 (1998).
- 13G. S. Zhdanov and N. G. Sevastyanov, "Crystal Structure of Boron Carbide (B<sub>4</sub>C)," *Dokl. Akad. Nauk. SSSR*, **32**, 832 (1941).
- 14H. K. Clark and J. L. Hoard, "The Crystal Structure of Boron Carbide," *J. Am. Chem. Soc.*, **65**, 2115–9 (1943).
- 15G. S. Zhdanov, N. N. Zhuravlev, and L. S. Zevin, "Roentgenographic Ordering of Structure in Boron Carbide," *Dokl. Akad. Nauk. SSSR*, **92** [4] 767–8 (1953).
- 16G. N. Samsonov, N. N. Zhuravlev, and I. G. Amnuel, "Physicochemical Properties of Boron-Carbon Alloys," *Fiz. Met. Metalloved.*, **3** [2] 309–13 (1956).
- 17A. S. Shtenberg, V. A. Raduchev, V. V. Denisevich, V. I. Ponomarev, S. S. Mamyan, and I. A. Kanayev, "Boron Carbide Single Crystal Growing Using Direct High-Frequency Melting in Cold Vessel," *Dokl. Akad. Nauk. SSSR*, **317** [2] 370–4 (1991).
- 18M. Bouchacourt and F. Thevenot, "The Melting of Boron Carbide and the Homogeneity Range of the Boron Carbide Phase," *J. Less-Common Met.*, **67**, 327–31 (1979).
- 19M. Bouchacourt and F. Thevenot, "Analytical Investigations in the BC System," *J. Less-Common Met.*, **82**, 219–26 (1981).
- 20L. B. Ekblom and C. O. Amundin, "Microstructural Evaluations of Sintered Boron Carbides with Different Compositions"; pp. 237–43 in *Science of Ceramics*, Vol. 11, Edited by R. Carlsson and S. Karlsson. Swedish Ceramic Society, Stockholm, 1981.
- 21M. Beauvy, "Stoichiometric Limits of Carbon-Rich Boron Carbide Phases," *J. Less-Common Met.*, **90** [2] 169–75 (1983).
- 22K. A. Schwetz and P. Karduck, "Investigations in the Boron-Carbon System with the Aid of Electron Probe Microanalysis"; pp. 405–13 in *Boron-Rich Solids*. Vol. 231, Edited by D. Emin, T. Aselage, C. L. Beckel, A. C. Switendick, and B. Morosin. American Institute of Physics, New York, 1991.
- 23D. Gosset and M. Colin, "Boron Carbides of Various Compositions: An Improved Method for X-Ray Characterization," *J. Nucl. Mater.*, **183**, 161–73 (1991).
- 24P. S. Kisly, M. A. Kuzenkova, N. I. Bodnaruk, and B. L. Grabchuk, *Karbid Bora (Boron Carbide)*, pp. 216. Naukova Dumka, Kiev, 1988.
- 25S. V. Konovalikhin and V. I. Ponomarev, "Carbon in Boron Carbide: The Crystal Structure of B<sub>11.4</sub>C<sub>3.6</sub>," *Russ. J. Inorg. Chem.*, **54** [2] 197–203 (2009).
- 26R. D. Allen, "The Solid Solution Series Boron – Boron Carbide," *J. Am. Chem. Soc.*, **75**, 3582 (1953).
- 27V. I. Matkovich, "Interstitial Compounds of Boron," *J. Am. Chem. Soc.*, **83**, 1804 (1961).
- 28V. I. Matkovich, "Extension of the Boron-Carbon Homogeneity Range," *J. Less-Common Met.*, **47**, 39 (1976).
- 29G. Will and K. H. Kossobutski, "An X-Ray Structure Analysis of Boron Carbide, B<sub>13</sub>C<sub>2</sub>," *J. Less-Common Met.*, **44**, 87 (1976).
- 30M. Bouchacourt and F. Thevenot, "The Properties and Structure of the Boron Carbide Phase," *J. Less-Common Met.*, **82**, 227–35 (1981).
- 31B. Morosin, A. W. Mullendore, D. Emin, and G. A. Slack, "Rhombohedral Crystal Structure of Compounds Containing Boron-Rich Icosahedra"; pp. 70–86 in *Boron-Rich Solids. AIP Conf. Proc.*, Vol. 140, Edited by D. Emin, T. Aselage, C. L. Beckel, I. A. Howard, and C. Wood. American Institute of Physics, New York, 1986.
- 32A. C. Larson, "Comments Concerning the Crystal Structure of B<sub>4</sub>C"; pp. 109–13 in *Boron-Rich Solids. AIP Conf. Proc.*, Vol. 140, Edited by D. Emin, T. Aselage, C. L. Beckel, I. A. Howard, and C. Wood. American Institute of Physics, New York, 1986.
- 33T. L. Aselage and R. G. Tissot, "Lattice Constants of Boron Carbide," *J. Am. Ceram. Soc.*, **75** [8] 2207–12 (1992).
- 34G. H. Kwei and B. Morosin, "Structures of the Boron-Rich Carbides from Neutron Powder Diffraction: Implications for the Nature of the Inter-Icosahedral Chains," *J. Phys. Chem.*, **100**, 8031–9 (1996).
- 35D. R. Armstrong, J. Balland, P. G. Pukins, and A. Kirsch, "The Nature of the Chemical Bonding in Boron Carbide. IV. Electronic Band Structure of Boron Carbide, B<sub>12</sub>C<sub>2</sub>, and Three Models of the Structure B<sub>12</sub>C<sub>3</sub>," *Acta Cryst. B*, **39**, 324–9 (1983).
- 36D. Emin, "Structure and Single-Phase Regime of Boron Carbides," *Phys. Rev. B*, **38** [9] 6041–55 (1988).
- 37D. M. Bylander, L. Kleinman, and S. B. Lee, "Self-Consistent Calculations of the Energy Bands and Bonding Properties of B<sub>12</sub>C<sub>3</sub>," *Phys. Rev. B*, **42** [2] 1394–403 (1990).
- 38D. M. Bylander and L. Kleinman, "Structure of B<sub>13</sub>C<sub>2</sub>," *Phys. Rev. B*, **43** [2] 1487–91 (1991).
- 39N. Vast, R. Lazzari, J. M. Besson, S. Baroni, and A. Dal Corso, "Atomic Structure and Vibrational Properties of Icosahedral  $\alpha$ -Boron and B<sub>4</sub>C Boron Carbide," *Comp. Mater. Sci.*, **17**, 127–32 (2000).
- 40G. Fanchini, J. W. McCauley, and M. Chhowalla, "Behavior of Disordered Boron Carbide Under Stress," *Phys. Rev. Lett.*, **97** [3] 035502 (2006).
- 41X. J. Guo, J. L. He, Z. Y. Liu, Y. J. Tian, J. Sun, and H. T. Wang, "Bond Ionicities and Hardness of B<sub>13</sub>C<sub>2</sub>-Like Structured B<sub>y</sub>X Crystals (X=C, N, O, P, As)," *Phys. Rev. B*, **73** [10] 104115 (2006).
- 42M. M. Balakrishnarajan, P. D. Pancharatna, and R. Hoffmann, "Structure and Bonding in Boron Carbide: The Invincibility of Imperfections," *New J. Chem.*, **31** [4] 473–85 (2007).
- 43J. E. Saal, S. Shang, and Z. K. Liu, "The Structural Evolution of Boron Carbide via Ab Initio Calculations," *Appl. Phys. Lett.*, **91** [23] 231915 (2007).
- 44V. I. Ivashchenko, V. I. Shevchenko, and P. E. A. Turchi, "First-Principles Study of the Atomic and Electronic Structures of Crystalline and Amorphous B<sub>4</sub>C," *Phys. Rev. B*, **80** [23] 235208 (2009).
- 45S. Aydin and M. Simsek, "Hypothetically Superhard Boron Carbide Structures with a B11C Icosahedron and Three-Atom Chain," *Phys. Status Solidi B*, **246** [1] 62–70 (2009).
- 46S. V. Konovalikhin and V. I. Ponomarev, "Estimation of the Upper Limit of Carbon Concentration in Boron Carbide Crystals," *Russ. J. Inorg. Chem. A*, **84** [8] 1445–8 (2010).
- 47A. H. Silver and P. J. Bray, "Nuclear Magnetic Resonance of Boron Carbide," *J. Chem. Phys.*, **31**, 247–53 (1959).
- 48T. V. Hynes and M. N. Alexander, "Nuclear Magnetic Resonance Study of  $\beta$ -Rhombohedral Boron and Boron Carbide," *J. Chem. Phys.*, **54**, 5296–310 (1971).
- 49T. M. Duncan, "The Distribution of Carbon in Boron Carbide: A <sup>13</sup>C Nuclear Magnetic Resonance Study," *J. Am. Chem. Soc.*, **106**, 2270–5 (1984).
- 50T. Harazono, Y. Hiroyama, and T. Watanabe, "Solid State NMR of B-11 and C-13 in Boron Carbide, B<sub>12</sub>C<sub>3</sub> and B-11 Enriched B<sub>12</sub>C<sub>3</sub>," *Bull. Chem. Soc. Jpn.*, **69** [9] 2419–23 (1996).
- 51K. L. Walters and G. L. Green, "B<sub>4</sub>C Structural Study"; pp. 14–16 in Quarterly Status Report on the Advanced Plutonium Fuels Program. Los Alamos National Laboratory, Los Alamos, 1970.
- 52H. L. Yakel, "The Crystal Structure of a Boron-Rich Boron Carbide," *Acta Cryst. B*, **31**, 1797–806 (1975).
- 53H. Stein, T. L. Aselage, and D. Emin, "Infrared Absorption in Boron Carbides: Dependence on Isotopes and Carbon Concentration"; pp. 322–25 in *Boron-Rich Solids. AIP Conf. Proc.*, Vol. 231, Edited by D. Emin, T. Aselage, C. L. Beckel, A. C. Switendick, and B. Morosin. American Institute of Physics, New York, 1991.
- 54U. Kuhlmann, H. Werheit, and K. A. Schwetz, "Distribution of Carbon Atoms on the Boron Carbide Structure Elements," *J. Alloy. Compd.*, **189**, 249–58 (1992).
- 55H. Werheit, T. Au, R. Schmeichel, S. O. Shalamberidze, G. I. Kalandadze, and A. M. Eristavi, "IR-Active Phonons and Structure Elements of Isotope-Enriched Boron Carbide," *J. Solid State Chem.*, **154**, 79–86 (1999).
- 56H. Werheit, U. Kuhlmann, H. W. Rotter, and S. O. Shalamberidze, "Isotope Effects on the Phonon Modes in Boron Carbide," *J. Phys. Condens. Mat.*, **22** [39] 395401 (2010).
- 57D. R. Tallant, T. L. Aselage, A. N. Campbell, and D. Emin, "Boron Carbides: Evidence for Molecular Level Disorder," *J. Non-Cryst. Solids*, **106** [1–3] 370–3 (1988).
- 58D. R. Tallant, T. L. Aselage, A. N. Campbell, and D. Emin, "Boron Carbide Structure by Raman Spectroscopy," *Phys. Rev. B*, **40** [8] 5649–56 (1989).

- <sup>59</sup>T. L. Aselage, D. R. Tallant, and D. Emin, "Isotope Dependencies of Raman Spectra of  $\text{B}_{12}\text{As}_2$ ,  $\text{B}_{12}\text{P}_2$ ,  $\text{B}_{12}\text{O}_2$ , and  $\text{B}_{12+x}\text{C}_{3-x}$ : Bonding of Intericosahedral Chains," *Phys. Rev. B*, **56** [6] 3122–9 (1997).
- <sup>60</sup>U. Kuhlmann and H. Werheit, "Raman Effect of Boron Carbide ( $\text{B}_{4.5}\text{C}$  to  $\text{B}_{10.37}\text{C}$ )," *J. Alloy. Compd.*, **205**, 87–91 (1994).
- <sup>61</sup>H. Werheit, H. W. Rotter, F. D. Meyer, H. Hillebrecht, S. O. Shalamberidze, T. G. Abzianidze, and G. G. Esadze, "FT-Raman Spectra of Isotope-Enriched Boron Carbide," *J. Solid State Chem.*, **177**, 569–74 (2004).
- <sup>62</sup>Y. J. Feng, G. T. Seidler, J. O. Cross, A. T. Macrander, and J. J. Rehr, "Role of Inversion Symmetry and Multipole Effects in Nonresonant X-Ray Raman Scattering from Icosahedral  $\text{B}_4\text{C}$ ," *Phys. Rev. B*, **69** [12] 125402 (2004).
- <sup>63</sup>R. S. Kumar, D. Dandekar, A. Leithe-Jasper, T. Tanaka, Y. M. Xiao, P. Chow, M. F. Nicol, and A. L. Cornelius, "Inelastic X-Ray Scattering Experiments on  $\text{B}_4\text{C}$  Under High Static Pressures," *Diam. Relat. Mater.*, **19** [5–6] 530–2 (2010).
- <sup>64</sup>F. Mauri, N. Vast, and C. J. Pickard, "Atomic Structure of Icosahedral  $\text{B}_4\text{C}$  Boron Carbide from a First Principles Analysis of NMR Spectra," *Phys. Rev. Lett.*, **87** [8] 085506 (2001).
- <sup>65</sup>R. Lazzari, N. Vast, J. M. Besson, S. Baroni, and A. Dal Corso, "Atomic Structure and Vibrational Properties of Icosahedral  $\text{B}_4\text{C}$  Boron Carbide," *Phys. Rev. Lett.*, **83** [16] 3230–3 (1999).
- <sup>66</sup>D. Lee, P. J. Bray, and T. L. Aselage, "The NQR and NMR Studies of Icosahedral Borides," *J. Phys. Condens. Mat.*, **11** [22] 4435–50 (1999).
- <sup>67</sup>H. C. Longuet-Higgins and M. de V. Roberts, "The Electronic Structure of an Icosahedron of Boron Atoms," *Proc. R. Soc. London, A*, **230**, 110–9 (1955).
- <sup>68</sup>C. Wood and D. Emin, "Conduction Mechanism in Boron Carbide," *Phys. Rev. B*, **29** [8] 4582–7 (1984).
- <sup>69</sup>C. Wood, D. Emin, and P. E. Gray, "Thermal Conductivity of Boron Carbides," *Phys. Rev. B*, **31** [10] 6811–4 (1985).
- <sup>70</sup>M. Van Schilfgaarde and W. A. Harrison, "Electronic Structure of Boron," *J. Phys. Chem. Solids*, **46** [9] 1093–100 (1985).
- <sup>71</sup>O. Chauvet, D. Emin, L. Forro, T. L. Aselage, and L. Zuppiroli, "Spin Susceptibility of Boron Carbides: Dissociation of Singlet Small Bipolarons," *Phys. Rev. B*, **53** [21] 14450 (1996).
- <sup>72</sup>T. L. Aselage, D. Emin, S. S. McCready, and R. V. Duncan, "Large Enhancement of Boron Carbides' Seebeck Coefficients Through Vibrational Softening," *Phys. Rev. Lett.*, **81** [11] 2316–9 (1998).
- <sup>73</sup>T. L. Aselage, D. Emin, and S. S. McCready, "Bipolaron Hopping Conduction in Boron Carbides," *Phys. Status Solidi B*, **218** [1] 255–8 (2000).
- <sup>74</sup>T. L. Aselage, D. Emin, and S. S. McCready, "Conductivities and Seebeck Coefficients of Boron Carbides: Softening Bipolaron Hopping," *Phys. Rev. B*, **64** [5] 054302 (2001).
- <sup>75</sup>J. H. Gieske, T. L. Aselage and D. Emin, "Elastic Properties of Boron Carbides"; pp. 376–9 in *Boron-Rich Solids. AIP Conf. Proc.*, Vol. 231, Edited by D. Emin, T. Aselage, C. L. Beckel, A. C. Switendick, and B. Morosin. American Institute of Physics, New York, 1991.
- <sup>76</sup>T. L. Aselage and D. R. Tallant, "Association of Broad Icosahedral Raman Bands with Substitutional Disorder in  $\text{SiB}_3$  and Boron Carbide," *Phys. Rev. B*, **57** [5] 2675–8 (1998).
- <sup>77</sup>A. Kirfel, A. Gupta, and G. Will, "The Nature of the Chemical Bonding in Boron Carbide,  $\text{B}_{13}\text{C}_2$ . I. Structure Refinement," *Acta Cryst. B*, **35**, 1052 (1979).
- <sup>78</sup>H. L. Yakel, "Recent Developments in the Structural Crystallography of Boron and the Higher Borides"; pp. 97–108 in *Boron-Rich Solids. AIP Conf. Proc.*, Vol. 140, Edited by D. Emin, T. Aselage, C. L. Beckel, I. A. Howard, and C. Wood. American Institute of Physics, New York, 1986.
- <sup>79</sup>R. Schmechel and H. Werheit, "Correlation Between Structural Defects and Electronic Properties of Icosahedral Boron-Rich Solids," *J. Phys. Condens. Mat.*, **11**, 6803–13 (1999).
- <sup>80</sup>T. Ogitsu, F. Gygi, J. Reed, Y. Motome, E. Schwegler, and G. Galli, "Imperfect Crystal and Unusual Semiconductor: Boron, a Frustrated Element," *J. Am. Chem. Soc.*, **131** [5] 1903–9 (2009).
- <sup>81</sup>M. W. Chen, J. W. McCauley, J. C. LaSalvia, and K. J. Hemker, "Microstructural Characterization of Commercial Hot-Pressed Boron Carbide Ceramics," *J. Am. Ceram. Soc.*, **88** [7] 1935–42 (2005).
- <sup>82</sup>J. Lagrenaudie, "A Study of the Properties of Boron," *J. Phys.-Paris*, **14**, 14–8 (1953).
- <sup>83</sup>H. Werheit, H. Binnenbruck, and A. Hausen, "Optical Properties of Boron Carbide and Comparison with  $\beta$ -Rhombohedral Boron," *Phys. Status Solidi B*, **47**, 153–8 (1971).
- <sup>84</sup>H. Werheit, "On Excitons and Other Gap States in Boron Carbide," *J. Phys. Condens. Mat.*, **18** [47] 10655–62 (2006).
- <sup>85</sup>M. Calandra, N. Vast, and F. Mauri, "Superconductivity from Doping Boron Icosahedra," *Phys. Rev. B*, **69** [22] 224505 (2004).
- <sup>86</sup>H. Dekura, K. Shirai, and A. Yanase, "Metallicity of Boron Carbides at High Pressure," *J. Phys.: Conf. Ser.*, **215**, 012117 (2010).
- <sup>87</sup>L. Kleinman, "Ab Initio Calculations of Boron and Its Carbides"; pp. 13–20 in *Boron-Rich Solids. AIP Conf. Proc.*, Vol. 231, Edited by D. Emin, T. Aselage, C. L. Beckel, A. C. Switendick, and B. Morosin. American Institute of Physics, New York, 1991.
- <sup>88</sup>L. Zuppiroli, N. Papandreou, and R. Kormann, "The Dielectric Response of Boron-Carbide Due to Hopping Conduction," *J. Appl. Phys.*, **70** [1] 246–52 (1991).
- <sup>89</sup>R. Schmechel and H. Werheit, "Evidence of the Superposition of Drude Type and Hopping Type Transport in Boron-Rich Solids," *J. Solid State Chem.*, **133** [1] 335–41 (1997).
- <sup>90</sup>H. Werheit and K. de Groot, "Metal-Insulator Transition in Boron Carbide," *Phys. Status Solidi B*, **97** [1] 229–38 (1980).
- <sup>91</sup>H. Werheit, K. de Groot, and W. Malkemper, "On the Metal-Insulator Transition of Boron Carbide," *J. Less-Common Met.*, **82**, 153–62 (1981).
- <sup>92</sup>G. A. Samara, H. L. Tardy, E. L. Venturini, T. L. Aselage, and D. Emin, "AC Hopping Conductivities, Dielectric-Constants, and Reflectivities of Boron Carbides," *Phys. Rev. B*, **48** [3] 1468–77 (1993).
- <sup>93</sup>D. Emin, "Electronic Transport in Boron Carbides"; pp. 189–205 in *Boron-Rich Solids. AIP Conf. Proc.*, Vol. 140, Edited by D. Emin, T. Aselage, C. L. Beckel, I. A. Howard, and C. Wood. American Institute of Physics, New York, 1986.
- <sup>94</sup>I. A. Howard, C. L. Beckel, and D. Emin, "Bipolarons in Boron Icosahedra," *Phys. Rev. B*, **35** [6] 2929–33 (1987).
- <sup>95</sup>I. A. Howard, C. L. Beckel, and D. Emin, "Bipolarons in Boron-Rich Icosahedra: Effects of Carbon Substitution," *Phys. Rev. B*, **35** [17] 9265–70 (1987).
- <sup>96</sup>D. Emin, "Electronic and Vibrational Hopping Transport in Boron Carbides"; pp. 65–76 in *Boron-Rich Solids. AIP Conf. Proc.*, Vol. 231, Edited by D. Emin, T. Aselage, C. L. Beckel, A. C. Switendick, and B. Morosin. American Institute of Physics, New York, 1991.
- <sup>97</sup>G. A. Samara, D. Emin, and C. Wood, "Pressure and Temperature Dependences of the Electronic Conductivity of Boron Carbides," *Phys. Rev. B*, **32** [4] 2315–8 (1985).
- <sup>98</sup>L. J. Azevedo, E. L. Venturini, D. Emin, and C. Wood, "Magnetic Susceptibility Study of Boron Carbides," *Phys. Rev. B*, **32** [12] 7970–2 (1985).
- <sup>99</sup>H. Werheit, "Are There Bipolarons in Icosahedral Boron-Rich Solids?" *J. Phys. Condens. Mat.*, **19** [18] 186207 (2007).
- <sup>100</sup>R. Franz and H. Werheit, "Jahn-Teller Effect of the  $\text{B}_{12}$  Icosahedron and its General Influence on the Valence Band Structures of Boron-Rich Solids," *Europhys. Lett.*, **9** [2] 145–50 (1989).
- <sup>101</sup>H. Werheit, "Present Knowledge of Electronic Properties and Charge Transport of Icosahedral Boron-Rich Solids," *J. Phys.: Conf. Ser.*, **176** [1] 012019 (2009).
- <sup>102</sup>J. Larruquet and R. A. M. Keski-Kuha, "Optical Properties of Hot-Pressed  $\text{B}_4\text{C}$  in the Extreme Ultraviolet," *Appl. Optics*, **39** [10] 1537–40 (2000).
- <sup>103</sup>H. Werheit, C. Janowitz, R. Schmechel, T. Tanaka, and Y. Ishizawa, "Interband Critical Points of Some Icosahedral Boron-Rich Solids," *J. Solid State Chem.*, **133** [1] 132–9 (1997).
- <sup>104</sup>H. Werheit, M. Laux, U. Kuhlmann, and R. Telle, "Optical Interband Transitions of Boron Carbide," *Phys. Status Solidi B*, **172**, K81–6 (1991).
- <sup>105</sup>H. Werheit, A. Leithe-Jasper, T. Tanaka, H. W. Rotter, and K. A. Schwegert, "Some Properties of Single-Crystal Boron Carbide," *J. Solid State Chem.*, **177**, 575–9 (2004).
- <sup>106</sup>R. Schmechel, H. Werheit, T. U. Kampen, and W. Mönch, "Photoluminescence of Boron Carbide," *J. Solid State Chem.*, **177**, 566–8 (2004).
- <sup>107</sup>H. Werheit, H. W. Rotter, S. Shalamberidze, A. Leithe-Jasper, and T. Tanaka, "Gap-State Related Photoluminescence in Boron Carbide," *Phys. Status Solidi B*, **177** [5], 1275–9 (2011).
- <sup>108</sup>H. Werheit, V. Filipov, U. Schwarz, M. Armbruster, A. Leithe-Jasper, T. Tanaka, and S. O. Shalamberidze, "On Surface Raman Scattering and Luminescence Radiation in Boron Carbide," *J. Phys. Condens. Mat.*, **22** [4] 045401 (2010).
- <sup>109</sup>K. Shirai and S. Emura, "Lattice Vibrations and the Bonding Nature of Boron Carbide," *J. Phys. Condens. Mat.*, **8**, 10919–29 (1996).
- <sup>110</sup>B. S. Abbott and C. L. Beckel, "Vibrational Analysis of  $\text{B}_4\text{C}$ "; pp. 344–6 in *Boron-Rich Solids. AIP Conf. Proc.*, Vol. 231, Edited by D. Emin, T. Aselage, C. L. Beckel, A. C. Switendick, and B. Morosin. American Institute of Physics, New York, 1991.
- <sup>111</sup>K. Shirai and H. Katayama-Yoshida, "Effects of the Geometries of Boron-Rich Crystals on the Lattice Dynamics," *J. Solid State Chem.*, **154**, 20–5 (2000).
- <sup>112</sup>K. Shirai and S. Emura, "Lattice Vibrations of Boron Carbide," *J. Solid State Chem.*, **133**, 93–6 (1997).
- <sup>113</sup>U. Kuhlmann and H. Werheit, "On the Microstructure of Boron Carbide," *Solid State Commun.*, **83** [11] 849–52 (1992).
- <sup>114</sup>V. Domnick, Y. Gogotsi, M. Trenary, and T. Tanaka, "Nanoindentation and Raman Spectroscopy Studies of Boron Carbide Single Crystals," *Appl. Phys. Lett.*, **81** [20] 3783–5 (2002).
- <sup>115</sup>H. Werheit, R. Schmechel, U. Kuhlmann, T. U. Kampen, W. Mönch, and A. Rau, "On the Reliability of the Raman Spectra of Boron-Rich Solids," *J. Alloys Comp.*, **291**, 28–32 (1999).
- <sup>116</sup>U. Kuhlmann and H. Werheit, "Improved Raman effect Studies on Boron Carbide ( $\text{B}_{4.5}\text{C}$ )," *Phys. Status Solidi B*, **175**, 85–92 (1993).
- <sup>117</sup>M. H. Mangnani, Y. Wang, F. Li, P. Zinin, and W. Rafanillo, "Elastic and Vibrational Properties of  $\text{B}_4\text{C}$  to 21 GPa"; pp. 945–8 in *Science and Technology of High Pressure*, Edited by M. H. Mangnani, W. J. Nellis, and M. F. Nicol. Universities Press, Hyderabad, India, 2000.
- <sup>118</sup>X. Q. Yan, Z. Tang, L. Zhang, J. J. Guo, C. Q. Jin, Y. Zhang, T. Goto, J. W. McCauley, and M. W. Chen, "Depressurization Amorphization of Single-Crystal Boron Carbide," *Phys. Rev. Lett.*, **102** [7] 075505 (2009).
- <sup>119</sup>J. J. Guo, L. Zhang, T. Fujita, T. Goto, and M. W. Chen, "Pressure-Induced Depolarization and Resonance in Raman Scattering of Single-Crystalline Boron Carbide," *Phys. Rev. B*, **81** [6] 060102 (2010).
- <sup>120</sup>R. J. Nelmes, J. S. Loveday, R. M. Wilson, W. G. Marshall, J. M. Besson, S. Klotz, G. Hamel, T. L. Aselage, and S. Hull, "Observation of Inverted-Molecular Compression in Boron Carbide," *Phys. Rev. Lett.*, **74** [12] 2268–71 (1995).
- <sup>121</sup>G. Fanchini, V. Gupta, A. B. Mann, and M. Chhowalla, "In Situ Monitoring of Structural Changes in Boron Carbide Under Electric Fields," *J. Am. Ceram. Soc.*, **91** [8] 2666–9 (2008).
- <sup>122</sup>T. Fujii, Y. Mori, H. Hyodo, and K. Kimura, "X-Ray Diffraction Study of  $\text{B}_4\text{C}$  Under High Pressure," *J. Phys. Conf. Ser.*, **215**, 012011 (2010).

- <sup>123</sup>B. A. Weinstein and G. J. Piermarini, "Raman Scattering and Phonon Dispersion in Si and GaP at Very High Pressure," *Phys. Rev. B*, **12** [4] 1172–86 (1975).
- <sup>124</sup>N. Binggeli and J. R. Chelikowsky, "Elastic Instability in Alpha-Quartz Under Pressure," *Phys. Rev. Lett.*, **69** [15] 2220–3. (1992).
- <sup>125</sup>S. L. Chaplot and S. K. Sikka, "Molecular-Dynamics Simulation of Pressure-Induced Crystalline-To-Amorphous Transition in Some Corner-Linked Polyhedral Compounds," *Phys. Rev. B*, **47** [10] 5710–4. (1993).
- <sup>126</sup>D. W. Dean, R. M. Wentzcovitch, N. Keskar, J. R. Chelikowsky, and N. Binggeli, "Pressure-Induced Amorphization in Crystalline Silica: Soft Phonon Modes and Shear Instabilities in Coesite," *Phys. Rev. B*, **61** [5] 3303–9 (2000).
- <sup>127</sup>S. P. Dodd, G. A. Saunders, and B. James, "Temperature and Pressure Dependences of the Elastic Properties of Ceramic Boron Carbide ( $B_4C$ )," *J. Mater. Sci.*, **37**, 2731–6 (2002).
- <sup>128</sup>A. C. Ferrari and J. Robertson, "Interpretation of the Raman Spectra of Disordered and Amorphous Carbon," *Phys. Rev. B*, **61** [20] 14095–107 (2000).
- <sup>129</sup>F. Tuinstra and J. L. Koenig, "Raman Spectrum of Graphite," *J. Chem. Phys.*, **53**, 1126–30 (1970).
- <sup>130</sup>A. C. Larson and D. T. Cromer, "Reexamination of the Crystal Structure of  $B_4C$ ," *Acta Cryst. A*, **28**, S53 (1972).
- <sup>131</sup>G. Will, A. Kirfel, and A. Gupta, "Is the Concept of Boron Icosahedra in Boron Carbide Correct?" *J. Less-Common Met.*, **67**, 13–8 (1979).
- <sup>132</sup>D. Emin, "Icosahedral Boron-Rich Solids," *Phys. Today*, **20** [1] 55–62 (1987).
- <sup>133</sup>K. Shirai, A. Masago, and H. Katayama-Yoshida, "High-Pressure Properties Of Icosahedron-Based Solid Borons," *Phys. Status Solidi B*, **241** [14] 3161–7 (2004).
- <sup>134</sup>D. R. Tallant, T. L. Aselage, and D. Emin, "Structure of Icosahedral Borides by Raman Spectroscopy"; pp. 301–11 in *Boron-Rich Solids. AIP Conf. Proc.*, Vol. 231, Edited by D. Emin, T. Aselage, C. L. Beckel, A. C. Switendick, and B. Morosin. American Institute of Physics, New York, 1991.
- <sup>135</sup>S. B. Lee, D. M. Bylander, and L. Kleinman, "Elastic Moduli of B-12 and its Compounds," *Phys. Rev. B*, **45** [7] 3245–7 (1992).
- <sup>136</sup>K. J. McClellan, F. Chu, J. M. Roper, and I. Shindo, "Room Temperature Single Crystal Elastic Constants of Boron Carbide," *J. Mater. Sci.*, **36** [14] 3403–7 (2001).
- <sup>137</sup>K. A. Schwetz and W. Grellner, "The Influence of Carbon on the Microstructure and Mechanical Properties of Sintered Boron Carbide," *J. Less Common Met.*, **82**, 37–47 (1981).
- <sup>138</sup>S. R. Murthy, "Elastic Properties of Boron Carbide," *J. Mater. Sci. Lett.*, **4** [5] 603–5 (1985).
- <sup>139</sup>M. Beauvy, "Propriétés mécaniques du carbure de bore fritte," *Rev. Int. Hautes Temp.*, **19**, 301–10 (1982).
- <sup>140</sup>K. Niihara, A. Nakahira, and T. Hirai, "The Effect of Stoichiometry on Mechanical Properties of Boron Carbide," *J. Am. Ceram. Soc.*, **67** [1] C13–4 (1984).
- <sup>141</sup>X. Q. Yan, W. J. Li, T. Goto, and M. W. Chen, "Raman Spectroscopy of Pressure-Induced Amorphous Boron Carbide," *Appl. Phys. Lett.*, **88**, 131905 (2006).
- <sup>142</sup>M. Bouchacourt and F. Thevenot, "Etudes sur le carbure de bore. I. Métallographie et microdureté Knoop du carbure de bore," *J. Less-Common Met.*, **59**, 119–30 (1978).
- <sup>143</sup>M. Bougoin, F. Thevenot, F. Dubois, and G. Fantozzi, "Synthèse et caractérisation de céramiques denses en carbure de bore," *J. Less Common Met.*, **114**, 257–71 (1985).
- <sup>144</sup>H. Lee and R. F. Speyer, "Hardness and Fracture Toughness of Pressureless-Sintered Boron Carbide ( $B_4C$ )," *J. Am. Ceram. Soc.*, **85** [5] 1291–3 (2002).
- <sup>145</sup>N. K. Bourne, "Shock-Induced Brittle Failure of Boron Carbide," *Proc. R. Soc. Lon. A*, **458**, 1999–2006 (2002).
- <sup>146</sup>T. J. Vogler, W. D. Reinhart, and L. C. Chhabildas, "Dynamic Behavior of Boron Carbide," *J. Appl. Phys.*, **95** [8] 4173–83 (2004).
- <sup>147</sup>T. Mashimo, Y. Hanaoka, and K. Nagayama, "Elastoplastic Properties Under Shock Compression of  $Al_2O_3$  Single Crystal and Polycrystal," *J. Appl. Phys.*, **63** [2] 327–36 (1988).
- <sup>148</sup>W. D. Reinhart, L. C. Chhabildas, and T. J. Vogler, "Investigating Phase Transitions and Strength in Single-Crystal Sapphire Using Shock-Reshock Loading Techniques," *Int. J. Impact Eng.*, **33** [1–12] 655–69 (2006).
- <sup>149</sup>N. Bourne, J. Millett, Z. Rosenberg, and N. Murray, "On the Shock Induced Failure of Brittle Solids," *J. Mech. Phys. Solids*, **46** [10] 1887–908 (1998).
- <sup>150</sup>D. P. Dandekar, W. D. Reinhart, and L. C. Chhabildas, "Reshock Behavior of Silicon Carbide," *J. Phys. IV*, **110**, 827–31 (2003).
- <sup>151</sup>T. J. Vogler, W. D. Reinhart, L. C. Chhabildas, and D. P. Dandekar, "Hugoniot and Strength Behavior of Silicon Carbide," *J. Appl. Phys.*, **99** [2] 023512. (2006).
- <sup>152</sup>W. D. Reinhart and L. C. Chhabildas, "Strength Properties of Coors AD995 Alumina in the Shocked State," *Int. J. of Impact Eng.*, **29** [110] 601–19 (2003).
- <sup>153</sup>M. L. Wilkins, *Third Progress Report of Light Armor Program*. Lawrence Livermore National Laboratory, University of California, CA, Report No. UCDES0460, 1968.
- <sup>154</sup>R. G. McQueen, S. P. Marsh, J. W. Taylor, J. N. Fritz, and W. J. Carter, "The Equation of State of Solids from Shock Wave Studies"; pp. 239–417 in *High-Velocity Wave Phenomena*, Edited by R. Kinslow. Academic Press, New York, 1970.
- <sup>155</sup>M. N. Pavlovskii, "Shock Compressibility of Six Very Hard Substances," *Sov. Phys. Solid State*, **12**, 1736–7. (1971).
- <sup>156</sup>W. H. Gust and E. B. Royce, "Dynamic Yield Strengths of  $B_4C$ ,  $BeO$ , and  $Al_2O_3$  Ceramics," *J. Appl. Phys.*, **42** [1] 276–95 (1971).
- <sup>157</sup>D. E. Grady, "Shock-Wave Strength Properties of Boron Carbide and Silicon Carbide," *J. Phys. IV*, **4**, 385–91 (1994).
- <sup>158</sup>Y. Zhang, T. Mashimo, Y. Uemura, M. Uchino, M. Kodama, K. Shiba, T. Fukuo, M. Kikuchi, T. Kobayashi, and T. Sekine, "Shock Compression Behaviors of Boron Carbide ( $B_4C$ )," *J. Appl. Phys.*, **100** [11] 113536 (2006).
- <sup>159</sup>D. E. Grady, "Analysis of Shock and High-Rate Data for Ceramics: Application to Boron Carbide and Silicon Carbide"; Report No. 0778, for U.S. Army TACOM-TARDEC, Warren, MI, Applied Research Associates, Inc., Albuquerque, NM, 2002.
- <sup>160</sup>D. E. Grady, "Analysis of Shock and High-Rate Data for Ceramics: Equation of State Properties and Fragmentation in the Ballistic Environment"; Report No. L18637, for U.S. Army TACOM-TARDEC, Warren, MI, Applied Research Associates, Inc., Albuquerque, NM, 2009.
- <sup>161</sup>M. Chen, J. W. McCauley, and K. J. Hemker, "Shock-Induced Localized Amorphization in Boron Carbide," *Science*, **299** 1563–6 (2003).
- <sup>162</sup>D. Ge, V. Domnich, T. Juliano, E. A. Stach, and Y. Gogotsi, "Structural Damage in Boron Carbide Under Contact Loading," *Acta Mater.*, **52** [13] 3921–7 (2004).
- <sup>163</sup>D. Ghosh, G. Subhash, C. H. Lee, and Y. K. Yap, "Strain-Induced Formation of Carbon and Boron Clusters in Boron Carbide During Dynamic Indentation," *Appl. Phys. Lett.*, **91** [6] 061910 (2007).
- <sup>164</sup>D. Ghosh, G. Subhash, T. S. Sudarshan, R. Radhakrishnan, and X. L. Gao, "Dynamic Indentation Response of Fine-Grained Boron Carbide," *J. Am. Ceram. Soc.*, **90** [6] 1850–7 (2007).
- <sup>165</sup>M. Chen and J. W. McCauley, "Mechanical Scratching Induced Phase Transitions and Reactions of Boron Carbide," *J. Appl. Phys.*, **100** 123517 (2006).
- <sup>166</sup>I. Pócsik, M. Hundhausen, M. Koós, and L. Ley, "Origin of the D Peak in the Raman Spectrum of Microcrystalline Graphite," *J. Non-Cryst. Solids*, **227–230** 1083–6 (1998).
- <sup>167</sup>M. S. Dresselhaus, G. Dresselhaus, M. A. Pimenta, and P. C. Eklund, "Raman Scattering in Carbon Materials"; pp. 367–434 in *Analytical Applications of Raman Spectroscopy*, Edited by M. Pelletier. Blackwell Science, Oxford, UK, 1999.
- <sup>168</sup>V. Kulikovsky, V. Vorlicek, R. Bohac, R. Ctvrtilk, M. Stranyanek, A. Dejneka, and L. Jastrabik, "Mechanical Properties and Structure of Amorphous and Crystalline  $B_4C$  Films," *Diam. Relat. Mater.*, **18** [1] 27–33 (2009).
- <sup>169</sup>S. Reynaud, "Fabrication and Characterization of Carbon and Boron Carbide Nanostructured Materials"; Ph.D. Thesis, Rutgers, The State University of New Jersey, NJ, 2010.
- <sup>170</sup>V. Domnich and Y. Gogotsi, "Indentation-Induced Phase Transformations in Ceramics"; pp. 443–66 in *High-Pressure Surface Science and Engineering*, Edited by Y. Gogotsi and V. Domnich. Institute of Physics Publishing, Bristol and Philadelphia, 2004.
- <sup>171</sup>V. Domnich, Y. Gogotsi, and M. Trenary, "Identification of Pressure-Induced Phase Transformations Using Nanoindentation," *Mat. Res. Soc. Symp. Proc.*, **649**, Q8.9.1–6 (2001). □



Vladislav Domnich is a research associate at the Center for Ceramic Research at Rutgers University. He received a B.S./M.S. degree in applied physics from Kiev Polytechnic Institute in Ukraine, and a Ph. D. degree in mechanical engineering from the University of Illinois at Chicago. Prior to joining the research faculty at Rutgers, he worked at the Institute for Metal Physics in Kiev, Ukraine, and held post-doctoral appointments at Drexel University and Arkema Inc. His research interests involve synthesis, processing, and characterization of ceramics, and structural transformations in materials under contact loading. His current work focuses on investigation of structure-property relations in silicon carbide and boron carbide powders and dense bodies. His main expertise is in vibrational spectroscopy and nanomechanical characterization of materials. He has published over 20 papers and co-edited a book on high pressure surface science.



Sara Reynaud is a post doctoral associate in the group of Prof. Richard Haber at the Materials Science and Engineering Department at Rutgers University. She completed her Ph.D. study at Rutgers under the direction of Prof. Manish Chhowalla. She received her B.S. and M.S. degrees from the University of Naples in Italy. Dr. Reynaud has published 4 papers and 3 more papers are in preparation. Following her M.S. degree, she spent one year working as an intern for the polymer branch of Arkema Inc., where she strengthened her knowledge in rheology and mechanical testing. Her Ph.D. research at Rutgers focused on the fabrication and characterization of nanostructured ceramics with particular attention to carbon based materials. Her laboratory work involved the preparation of boron carbide thin films by magnetron sputtering and arc discharge. Her main research interests are in engineering novel structures able to enhance or eventually tune the properties of materials aimed at cutting-edge technologies. More recently, she has been investigating the effect of industrial processing on the microstructure of both organic and inorganic materials at multiple scales.



Richard Haber is a professor of Material Science and Engineering at Rutgers University. He is also the Director of the Center for Ceramic Research, part of the NSF I/UCRC Ceramic, Composite and Optical Material Center. Prof. Haber also directs the US Army Material Center of Excellence in Lightweight Materials for Vehicle Protection. He received his BS, MS and PhD degrees in Ceramic Engineering at Rutgers and has been on the faculty for 26 years. He is a Fellow of the American Ceramic Society and past Vice President. He has received the Schwarzwaldcer PACE and John Marquis Awards. His research interests are in the synthesis and processing of ceramics. Most recently his research has focused on boron carbide powder synthesis and grain boundary engineering in opaque and transparent ceramics. He has published over 140 papers in a wide range of topics including powders, synthesis, processing, non destructive analysis and tailored microstructures in ceramics.



Manish Chhowalla is a Professor and Associate Chair of the Materials Science and Engineering Department at Rutgers University. He is also the Director of Nanotechnology for Clean Energy NSF IGERT Program and the Donald H Jacobs Chair in Applied Physics (2009–2011). From June 2009–July 2010 he was a Professor in the Department of Materials at Imperial College London. He has won the NSF CAREER Award for young scientists as well as the Sigma Xi Outstanding Young Investigator for the Mid Atlantic Region. Before Rutgers, he was a Royal Academy of Engineering Postdoctoral Research Fellow at the University of Cambridge after completing his Ph.D. in Electrical Engineering there. Prior to his PhD, he worked for Multi-Arc Inc. (now Ion Bond) where he developed one of the first applications of “amorphous diamond” thin films. His technological interests are in the synthesis and characterization of novel carbon materials and their incorporation into devices for electrical, optical and mechanical applications. Fundamentally, he is interested in understanding the role of disorder in determining material properties. His research topics presently include investigation of the opto-electronic properties of graphene and carbon nanotubes, organic memory and photovoltaic devices, structural properties of boron carbide, and deposition of carbide and nitride thin films. He has over 120 publications with over 6500 citations on these topics and has given >90 invited/keynote/plenary lectures. He has also served on organizing committees for numerous international conferences.